Pacific Northwest
NATIONAL LABORATORY

Proudly Operated by **Battelle** *Since 1965*

Solid State Characterizations of Long-Term Leached Cast Stone Monoliths

September 2016

RM Asmussen   N Washton
CI Pearce   M Bowden
KE Parker   AR Lawter
B Miller   E McElroy
B Lee   RJ Serne
E Buck

U.S. DEPARTMENT OF
ENERGY

DISCLAIMER

This report was prepared as an account of work sponsored by an agency of the United States Government. Neither the United States Government nor any agency thereof, nor Battelle Memorial Institute, nor any of their employees, makes **any warranty, express or implied, or assumes any legal liability or responsibility for the accuracy, completeness, or usefulness of any information, apparatus, product, or process disclosed, or represents that its use would not infringe privately owned rights**. Reference herein to any specific commercial product, process, or service by trade name, trademark, manufacturer, or otherwise does not necessarily constitute or imply its endorsement, recommendation, or favoring by the United States Government or any agency thereof, or Battelle Memorial Institute. The views and opinions of authors expressed herein do not necessarily state or reflect those of the United States Government or any agency thereof.

Solid State Characterizations of Long-Term Leached Cast Stone Monoliths

RM Asmussen
CI Pearce
KE Parker
B Miller
B Lee
E Buck

N Washton
M Bowden
A Lawter
E McElroy
RJ Serne

September 2016

Pacific Northwest National Laboratory
Richland, Washington 99352

Executive Summary

This report describes the results from the solid phase characterization of six Cast Stone monoliths from the extended leach tests recently reported on (Serne et al. 2016),that were selected for characterization using multiple state-of-the-art approaches. The Cast Stone samples investigated were leached for > 590 d in the EPA Method 1315 test then archived for > 390 d in their final leachate. After reporting the long term leach behavior of the monoliths (containing radioactive ^{99}Tc and stable ^{127}I spikes and for original Westsik et al. 2013 fabricated monoliths, ^{238}U), it was suggested that physical changes to the waste forms and a depleting inventory of contaminants of potential concern may mean that effective diffusivity calculations past 63 d should not be used to accurately represent long-term waste form behavior. These novel investigations, in both length of leaching time and application of solid state techniques, provide an initial arsenal of techniques which can be utilized to perform such Cast Stone solid phase characterization work, which in turn can support upcoming performance assessment maintenance. The work was performed at Pacific Northwest National Laboratory (PNNL) for Washington River Protection Solutions (WRPS) to characterize several properties of the long-term leached Cast Stone monolith samples:

1. Radionuclide distribution in the long-term leached Cast Stone. Using single particle digital autoradiography imaging of Cast Stone cross sections, two distributions of ^{99}Tc were observed: a) congregation in a ring near the outer edge of the monolith, and b) isolation in discrete "hot spots". ^{238}U was also observed to be isolated in discrete locations in the one monolith cross section that contained ^{238}U. These observations are of high interest as cementitious waste forms are assumed to have homogenous distribution of radionuclides, however this is not the case. As well, being able to identify locations where radionuclides are concentrated will allow more effective future characterization of the radionuclide-bearing phases in the waste form and their behavior over time.

2. Ingress of CO_3^{2-} into the Cast Stone monoliths. Phenolphthalein staining of monoliths sectioned under anoxic conditions was performed to identify the ingress of CO_3^{2-}, as measured by pH changes, into the monolith from the outer wall to the interior. The four monoliths analyzed showed staining all the way to the outer wall of the monolith. This indicates that the monolith retained high alkalinity and ingress of CO_3^{2-} was not sufficient to reduce substantially the pH. However, Cast Stone leached in Hanford vadose zone pore water (VZPW), exhibited a white precipitate evenly distributed to a depth of ~ 5 mm inward from the monoliths' outer surface. In this "outer skin" region, the white precipitate deposited in the pores reduced the porosity to some extent. X-ray diffraction (XRD) analyses showed that the white precipitate was mainly ettringite with some calcium carbonate. It is postulated that CO_3^{2-} (or CO_2 gas) does enter the monoliths via pores and cracks, leading to precipitation of carbonates and initiating the growth of ettringite through reaction with SO_4^{2-}, which is present both in the monolith from the LAW simulant and in the VZPW. However, the extent of CO_3^{2-} ingress is not significant enough to overcome all the alkalinity of the solidified Cast Stone. This finding is of importance as it gives needed insight into the behaviour of carbonate in long-term leached Cast Stone.

3. Ingress of O_2 into the Cast Stone monoliths. Short-term DIW leach testing was performed on monolith samples sectioned under anoxic conditions to determine ingress of O_2. The method used was based on previous studies (Almond et al. 2012, Langton et al. 2013a, Langton et al. 2013b). Slightly less Tc (5%-13%) was leached from samples taken near the monoliths' outer walls

compared to the amount of Tc leached from samples taken within the monolith interior core (> 20 mm inward from the monolith walls (11% - 21%)). For Cr, the releases were much smaller (≤0.5%) with less Cr leached from samples taken near the monolith wall compared with samples taken from the monoliths' interior core. These results suggest that ingress of O_2 into water-saturated monoliths is likely minimal after > 1000 d exposure to solution in the open atmosphere during the EPA Method 1315 leach testing and subsequent wet storage. This finding bodes well for long-term performance of cementitious waste forms suggesting that they are able to retain redox sensitive species that are reduced to relatively insoluble species by the blast furnace slag over time under water saturated conditions. It is unclear without further testing if similar behaviour is expected in unsaturated conditions or in fractured/rubblized grouts, and upon waste form removal from saturated environments and exposure to the open atmosphere.

4. Mineralogical and chemical evolution of the Cast Stone. A clear change in the Al bonding environment was observed in the leached Cast Stone samples from the outer wall (Al in octahedral coordination) compared with the interior analyzed with nuclear magnetic resonance spectroscopy. X-ray diffraction spectroscopy (XRD) showed differences in the mineralogy between the monolith inner cores and their outer walls, suggesting that that mineral phases were transforming into more thermodynamically stable phases as leaching progressed. Electron microscopy imaging also showed that Tc was present on the monolith outer wall. From the structural NMR, XRD and microscopy data, it is clear that the Cast Stone mineralogy and chemical composition is evolving to produce heterogeneity between the monolith interior and the monolith's walls interface with the leach solution. This important finding confirms that the Cast Stone waste forms evolve over time and this may directly impact radionuclide retention.

The initial solid state characterization performed on the six selected Cast Stone monoliths show a general trend of a developing structural and chemical heterogeneity in the monoliths relative to the outer wall-solution interface. Further analysis of other remaining archived long-term leached monoliths is thus warranted to understand and confirm the trends observed, in hopes of being able to accurately predict the long-term performance of cementitious waste forms upon disposal. That is, these initial solid phase characterization studies have laid the groundwork to develop a systematic study of more of the remaining archived monoliths to understand the unique features documented in this report. Future efforts should address the following remaining questions/issues:

i) How does the radionuclide distribution within the monoliths change with leaching times? A second radiography imaging of leached monolith "pucks", after an initial imaging with radiography can show where Tc/U is most easily lost from and its migration within the monolith cross section.

ii) Compositional identification of Tc isolations in the Cast Stone is facilitated using the radiography map to focus SEM/EDS/XRF analyses on these Tc hot spot regions.

iii) For the monoliths studied in this work, all have one (and in some cases two) monoliths from the same batch archived in solution that can be characterized to confirm and perhaps more quantitatively measure the trends found in these scoping studies. Analyzing these additional monoliths will allow for insight into whether the trends observed are compositional effects, batch specific, monolith specific or due to the composition of the leachant. Also analyzing "un-leached" monoliths from similar monolith batches would provide a suitable control.

iv) A combination of radiography, SEM/EDS and XRF of "hot spots", NMR, XRD and XAS, along with further leaching of the imaged monoliths should be used in future solid phase characterization.

v) Short-term leach tests should be performed on similar pieces of the waste forms in both anoxic and aerobic environments and under both water saturated/unsaturated conditions followed by detailed solid phase characterization to determine the effect of exposure to air on the chemical and physical evolution of the Cast Stone. Additionally, upon removing a monolith from long-term leachate storage it would be beneficial to expose the monolith to the open atmosphere and observe any ingress of oxygen from the air to confirm the minimal oxygen ingress observed in our solution exposure tests.

Acknowledgments

Acronyms and Abbreviations

ASTM	American Society for Testing and Materials
BFS	blast furnace slag
BSE	backscattered electrons
CCD	charge coupled device
CMOS	complementary metal oxide semiconductor
COC	contaminant of concern
DDI	deionized water (18.2 MΩ·cm)
DIW	deionized water (building)
DOE	United States Department of Energy
DP	direct polarization
EDS	X-ray energy dispersive spectroscopy
EM	DOE Office of Environmental Management
EMSP	Environmental Management Science Program
EPA	United States Environmental Protection Agency
ETF	Effluent Treatment Facility
FA	fly ash
FY	fiscal year
HLW	high level waste
ICP-MS	inductively coupled plasma mass spectroscopy
ICP-OES	inductively coupled optical emission spectroscopy
IDF	Integrated Disposal Facility
iQid	ionizing-radiation quantum imaging detector
LAW	low activity waste
NW	Northwest
NMR	nuclear magnetic resonance spectroscopy
OPC	ordinary Portland cement
PA	performance assessment
PBS	phosphate buffered solution
PNNL	Pacific Northwest National Laboratory
PTFE	polytetrafluoroethylene
QA	quality assurance
QIIME	Quantitative Insights Into Microbial Ecology

R&D	research and development
SE	Southeast
SEM	scanning electron microscopy
SRNL	Savannah River National Laboratory
VZPW	vadose zone pore water
WRPS	Washington River Protection Solutions
WTP	Waste Treatment Plant
WWFTP	WRPS Waste Form Testing Program
XANES	X-ray absorption near edge structure
XAS	X-ray absorption spectroscopy
XRD	X-ray diffraction spectroscopy
XRF	X-ray fluorescence spectroscopy

Contents

Figures

Tables

1.0   Introduction

1.1   Program Overview

The U.S. Department of Energy (DOE) Hanford Site has177 underground single- and double-shell tanks that currently hold 56 million gallons of radioactive waste (Serne et al. 2016). Treatment of this waste will occur at the Hanford Tank Waste Treatment and Immobilization Plant (WTP), which is currently under construction. The wastes will be segregated into a small volume of high radioactivity high level waste (HLW) and a significant volume of lower radioactive low activity waste (LAW) to be disposed at the Hanford Site Integrated Disposal Facility (IDF). The HLW will be vitrified to form a glass based waste form for disposal at a yet to be determined Federal repository. Secondary waste streams produced as a result of WTP activities will also be treated with the candidate baseline technology is solidified as low temperature cementitious waste forms (also called grouts).

The LAW fraction will be vitrified as a borosilicate glass, however this presents challenges due to: (i) limited incorporation of key contaminants of concern (COC) (i.e. ^{99}Tc and ^{129}I) into the glass structure due to their volatility in the high-temperature vitrification process; and (ii) the quantity of LAW to be treated exceeds available vitrification capacity. A possible alternative for the disposal of excess LAW is solidification in a different waste form. Cementitious waste forms are a promising technology as their low fabrication temperature overcomes the volatility issue, thus lowering the cost burden associated with recycling key contaminants through the melter system to maximize their retention in the waste form (Westsik et al. 2013). Cast Stone, a grout mixture of 47 % blast furnace slag (BFS), 45% fly ash (FA) and 8 % ordinary Portland cement (OPC), has been studied in a serial approach, (through varying the dry blend ratio, simulant composition, liquid to dry blend ratio and inclusion of getters) over the past several years as a grout-based solidification technology for LAW. A similar mixture called saltstone (made of 45% BFS 45% FA and 10% OPC) is used to solidify LAW tank waste at the Savannah River Site (Cantrell et al. 2013).

Cast Stone was one of three supplemental immobilization technologies originally considered as part of a mission acceleration initiative to provide the necessary capacity to complete the Hanford tank waste cleanup mission in a timely manner (Raymond et al. 2004). It was noted that limited data were available on Cast Stone for the immobilization of Hanford LAW. This lack of data was the impetus for initiating the Cast Stone development program for Hanford LAW.

The Cast Stone development program began in fiscal year (FY) 2012 with work on projected waste streams from WTP and ETF. Enhancements to the Cast Stone performance, such as adding getters for Tc and I, are being pursued to further improve retention of key risk driver COC such that it could reasonably be considered as a supplemental immobilization technology for Hanford LAW. Any waste form under consideration for disposal at the IDF must pass rigorous testing to ensure acceptance criteria are met and that the long-term weathering behavior is understood with a strong technical basis. These waste form performance data are needed to support risk assessment and performance assessment (PA) analyses of the long-term environmental impact of waste disposal in the IDF. The PA is needed to satisfy both Washington State IDF Permit and DOE Order requirements.

Activities supporting the IDF PA require a long-term testing program. The main experimental investigations focus on (i) measuring release rates for contaminants over extended periods; (ii)

understanding the long-term evolution or weathering of Cast Stone/grout in the disposal environment; (iii) developing an understanding of the mechanism by which radionuclides and other contaminants are retained in the Cast Stone/grout, (iv) the mechanism(s) of release; (v) developing accelerated test methods and other test methods to characterize and predict the long-term performance of the Cast Stone/grout, and (vi) characterizing the release and subsequent transport properties of the key contaminants solidified in Cast Stone/grout (such as Tc, I, Cr) as water migrates through the disposal packages contained within IDF. The work done to date to support this venture has focused on measuring contaminant release rates; however, characterizing the evolution of the Cast Stone/grout solid phase with time is an integral part of accurately predicting its weathering behavior.

The leach testing of a select inventory of Cast Stone monoliths fabricated and used in previous leach tests (Westsik et al. 2013, Serne et al. 2016) was extended beyond the standard 63-d period suggested in U.S. Environmental Protection Agency (EPA) Method 1315 (EPA 2013). The long-term leached monolith samples were sampled at varying intervals over the past several years and the results from the liquid phase analyses are summarized in a recent report(Serne et al. 2016). In addition, long-term leach tests have generated a large inventory of leached monoliths that are available for detailed post-leaching solid phase characterization. Characterization of these leached monoliths provides a unique opportunity to obtain much needed information on Cast Stone waste form evolution over extended time periods including: (i) changes to the structure and mineralogy of the Cast Stone; (ii) changes in the distribution of contaminants within the monolith; and (iii) rate of ingress of carbonate and oxygen into the monolith. This information is valuable to PA support and is essential to understand the mechanism of release of contaminants from cementitious waste forms.

1.2 Objectives of This Task

The objective of this effort is to conduct focused post-reaction (extended leached) solid-phase characterization of leached Cast Stone monoliths to elucidate important contaminant release mechanisms that occur after years of leaching. The Cast Stone monoliths were precisely sectioned using a diamond bladed saw and specimens collected relative to the monolith outer wall. Identification of the minerals present in the leached Cast Stone under water saturated conditions as a function of leach time and distance from the monolith surface provides information on the evolution of monolith structure that occurs as a result of Cast Stone-leachant interaction. Similar monoliths were leached separately in deionized water (DIW) and simulated vadose zone pore water (VZPW) to provide insight into any potential problematic or advantageous effects associated with the actual disposal conditions in the IDF. Key data collected include

(i) the penetration depth of carbonation and oxidation fronts into Cast Stone monoliths using anoxic phenolphthalein staining and short-term DIW leach testing, respectively,

(ii) the mineralogy of both the cured Cast Stone before leaching and the secondary-minerals formed after long-term reaction with leachant solution, as a function of distance from the monolith surface using X-ray diffraction (XRD) spectroscopy, nuclear magnetic resonance spectroscopy (NMR) and electron microscopy,

(iii) the distribution of radionuclides within Cast Stone cross sections after extended leaching using single particle digital autoradiography.

1.3 Contents and Organization

The ensuing sections of this report describe the technical scope and approach of the testing program, presentation of the results, discussion of their impact, conclusions and identification of recommended future work. Appendix A contains the calculations from the oxidation front short- term leach testing. Appendix B contains tables of the sectioning details of the monoliths.

1.4 Quality Assurance

The Cast Stone monoliths used to conduct the solid state characterization studies were prepared and leached over several years (~590 days under EPA Method 1315 and > 300 days fully submerged in an aliquot of their final leachate) under several contract releases from Washington River Protection Solutions and DOE Headquarters Office of Environmental Management (EM). PNNL project 62745, (WRPS contract releases 36437-122 and 36437-134) funded preparation of the following monoliths: T10HCS-15HIS-3, T17LCS2-5HIA-6, T21LCS1-7.8HIS-4 and T14LCS2-7.8HIS-5. In the most recent report by Serne et al. (Serne et al. 2016), these monoliths were described as part of the Extended and Archived Suites. The Cast Stone monolith preparation details are described in test plan TP-62745-001. Leach testing of the Extended Suite of monoliths through the first 91 days of testing was conducted under project 62745. The leach testing of the Extended Suite of monoliths was continued beyond 91 days to a total of 252-257 days (up to the end of September 2013) with funding from the DOE EM-31 Support Program (EMSP) "Production and Long-term Performance of Low Temperature Waste Forms". The work was conducted under the Environmental Management Science Program (EMSP) Project Test Plan TP-EMSP-0011 and under the EMSP Quality Assurance Plan (QA-EMSP-001). The same EMSP funding supported the leach tests of the Archived Suite of monoliths up to September 2013. Beyond September 2013, the leach testing of both the Extended and Archived Suite of monoliths continued again with funding from WRPS as part of the Supplemental Immobilization of Hanford Low-Activity Waste (LAW) project (PNNL project 66596, WRPS contract release 36437-166). This work was done under the PNNL QA Plan *WRPS Waste Form Testing Program Quality Assurance Plan* (QA-WWFTP-001). Then in October 2014 the extended leach testing was funded by WRPS under PNNL project 68334 using the same QA requirements and documents.

The other monoliths studied, CS-T5-VZ-2 and CS-T5-DI-4, were prepared in June 2013 and long-term leach tested after 28 days curing and initially funded by the DOE EMSP "Production and Long-term Performance of Low Temperature Waste Forms". Serne et al. (2015, 2016) identified these monoliths as part of the Tc-Gluconate Suite. The leach testing of the Tc-Gluconate Suite of monoliths was conducted under the EMSP Project Test Plan TP-EMSP-0011 and under the EMSP Quality Assurance Plan (QA-EMSP-001). Leach testing was started in July 2013 and continued to September 2013 with the DOE

EMSP funding. Beyond September 2013, the leach testing continued with funding from WRPS as part of the Supplemental Immobilization of Hanford LAW project (PNNL project 66596, WRPS contract release 36437-166). This work was done under the PNNL QA Plan *WRPS Waste Form Testing Program Quality Assurance Plan* (QA-WWFTP-001). Then in October 2014 the extended leach testing of the Tc-Gluconate Suite of monoliths was funded under PNNL project 68334 using the same QA requirements and documents.

All research and development (R&D) work at PNNL is performed in accordance with PNNL's Laboratory-level Quality Management Program, which is based on a graded application of NQA-1-2000, *Quality Assurance Requirements for Nuclear Facility Applications*, to R&D activities. In addition to the PNNL-wide quality assurance (QA) controls, the QA controls of the WRPS Waste Form Testing Program (WWFTP) QA program were also implemented for the work. The WWFTP QA program consists of the WWFTP Quality Assurance Plan (QA-WWFTP-001) and associated QA-NSLW-numbered procedures that provide detailed instructions for implementing NQA-1 requirements for R&D work. The WWFTP QA program is based on the requirements of NQA-1-2008, *Quality Assurance Requirements for Nuclear Facility Applications*, and NQA-1a-2009, *Addenda to ASME NQA-1-2008 Quality Assurance Requirements for Nuclear Facility Applications*, graded on the approach presented in NQA-1-2008, Part IV, Subpart 4.2, "Guidance on Graded Application of Quality Assurance (QA) for Nuclear-Related Research and Development".

Performance of this work and preparation of this report were assigned the technology level "Applied Research" and were conducted in accordance with procedure QA-NSLW-1102, *Scientific Investigation for Applied Research.* All staff members contributing to the work have technical expertise in the subject matter and received QA training prior to performing quality-affecting work. The "Applied Research" technology level provides adequate controls to ensure that the activities were performed correctly. Use of both the PNNL-wide and WWFTP QA controls ensured that all client QA expectations were addressed in performing the work.

Records of all of the experimental work are filed with the records for the Supplemental Immobilization of Hanford LAW project and Secondary Waste Cast Stone (PNNL projects 66596 and 66334, respectively).

2.0 Technical Approach and Methods

2.1 Selection of Cast Stone Monoliths

Six Cast Stone monoliths from the extended EPA Method 1315 leach testing described in Serne et al. (Serne et al. 2016) that had been archived in their last leachate were chosen for further characterization in this report. All six monoliths were originally prepared using a dry blend comprised of the standard Cast Stone mix of 47 wt % BFS, 45 wt% class F FA and 8 wt% OPC. The monoliths contained radioactive ^{99}Tc and stable [127]I spikes and for monoliths fabricated by Westsik et al. (2013) [238]U. The monoliths were leached in DIW or VZPW, the composition of which is comprised of approximately 12 mM $CaSO_4 \cdot 2H_2O$, 1.7 mM NaCl, 0.4 mM $NaHCO_3$, 3.4 mM $NaNO_3$, 2.6 mM $MgSO_4$, 2.4 mM $MgCl_2 \cdot 6H_2O$, 0.7 mM KCl. Monolith ID's, fabrication details and report references are listed in Table 2-1 below:

Table 2-1 – History of Cast Stone monoliths characterized in this study.

Monolith ID	Short Name	Fabrication Report	BFS and FA Sources	Simulant Used	Water : Dry Mix Ratio	Spike	Leaching Start Date	Leaching End Date	Archive End Date	Leachant
CS-T5-VZ-2	T5-VZ	Serne et al. 2016	FA = NW BFS = SE	7.8 M Na average LAW simulant	0.60	Tc = 16 ppm	7/29/2013	2/18/2015	3/17/2016	VZPW
CS-T5-DI-4	T5-DI	Serne et al. 2016	FA = NW BFS = SE	7.8 M Na average LAW simulant	0.60	Tc = 16 ppm	7/29/2013	2/18/2015	3/17/2016	DIW
T10HCS1-5HIS-3	T10	Westsik et al. 2013	FA = NW BFS = NW	5 M Na High SO_4 LAW	0.60	Tc = 12 ppm I = 100 ppm	7/9/2013	2/19/2015	3/17/2016	VZPW
T14LCS2-7.8HIS-5	T14	Westsik et al. 2013	FA = SE BFS = SE	7.8 M Na High SO_4 LAW	0.40	Tc = 12 ppm I = 156 ppm	7/9/2013	2/19/2015	3/8/2016	VZPW
T17LCS2-5HIA-6	T17	Westsik et al. 2013	FA = SE BFS = SE	5.0 M Na High Al LAW	0.60	Tc = 12 ppm I = 100 ppm	7/9/2013	2/19/2015	3/17/2016	DIW
T21LCS1-7.8HIS-4	T21	Westsik et al. 2013	FA = SE BFS = NW	7.8 M Na High SO_4 LAW	0.60	Tc = 12 ppm I = 156 ppm	7/9/2013	2/19/2015	1/4/2016	VZPW

NW = Northwest Source
SE = Southeast Source

The monoliths from the Westsik et al. (2013) report also contained [238]U added to the various LAW simulants. These monoliths were removed from their leaching buckets on February 18-19, 2015 and stored submerged in their final leachate solution in polytetrafluoroethylene (PTFE) bottles (1L) prior to solid state characterization. T5-VZ and T5-DI were leached for 570 d before being transferred to the archive solution for an additional 393 d. T10 and T17 were leached for 590 d before the archive solution transfer for an additional 392 d. T14 was leached for 590 d before transferring to the archive solution for 381 d. T21 was leached for 590 d and archived for 319 d.

.

2.2 Sectioning of Cast Stone Monoliths

Following their removal from their final leachate, the Cast Stone monoliths were prepared for the solid state characterization using two approaches:

1) Fracturing the monolith using a manual benchtop press fitted with a pointed bit

2) Cutting the monolith with a dry diamond bladed saw (~ 1.58 mm thickness) with a Workforce Tile Saw THD550 inside an anoxic chamber under N_2/H_2 atmosphere to avoid or minimize Tc re-oxidation.

In method 1, for T14 and T21 monoliths, monoliths were removed from solution, measured and weighed, prior to fracturing with the manual press. These monoliths were not involved in oxidation front measurements and thus potential re-oxidation of Tc was not of concern. Each resulting fractured section was measured with calipers and segregated into "inner" and "outer" pieces to know the distance from the monolith wall where the inner section was collected.

In method 2, for the T5-DI, T5-VZ, T10 and T17 monoliths, monoliths were removed from solution, measured and weighed, prior to sectioning with a diamond-bladed saw in a glove bag with a N_2/H_2 atmosphere to minimize re-oxidation. Each cross-sectioned "hockey puck" was numbered based on position relative to the top of the monolith (Figure 2-1). Sectioning details for the monoliths can be found in Appendix B.

The pucks from the middle "C" section were further sectioned based on distance from the outer wall, measured using a ruler or calipers (± 5 mm). The sectioned pieces were given a new unique two digit ID, e.g. C3, A2 where the letter represents the disk i.e. vertical height position in the monolith, and the number represents the position of the slice, i.e. distance from the outer wall (Figure 2-1).
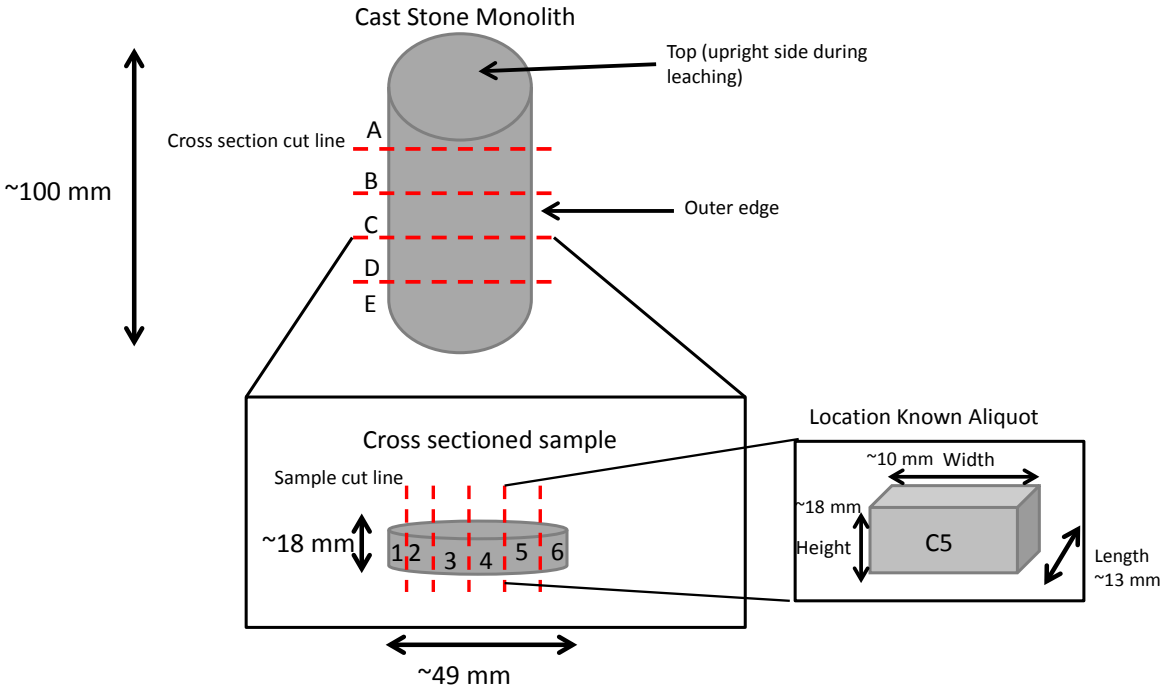
Figure 2-1 - Diagram showing the sectioning approach for the monoliths prepared via Method 2.

2.3 Phenolphthalein Staining

Phenolphthalein staining was used as a measure of carbonation ingress into the Cast Stone monoliths. The phenolphthalein indicator creates a deep reddish-purple color at pH ≥ 9.8 on the Cast Stone samples' surface. Below pH 9.8, the color varies from red to pink, and at pH ≤8 phenolphthalein is colorless. The pH of the initial cured Cast Stone is >10. Carbonation occurs because the calcium bearing phases present in the cured Cast Stone are attacked by dissolved carbon dioxide, from the air and VZPW, and converted to calcium carbonate, reducing the pH to <8. The depth of carbonation was measured as the distance from the monolith surface to the point where there was a visible change in color of the indicator, i.e. carbonation ingress corresponded to the area of the Cast Stone that remained colorless. The monoliths analyzed in this study were fabricated with caustic LAW simulants containing carbonate and this could lead to variability in the influence of CO_3 ingress changing overall pH compared with grouts fabricated with water or non-carbonate bearing simulants.

The entire bottom surface of disk B (see Figure 2-1) from selected monoliths was chosen for phenolphthalein staining in an anoxic glove bag to prevent any reaction with atmospheric CO_2 and O_2. Phenolphthalein stain (~1 mL, 1% phenolphthalein + 99 % ethyl alcohol), was pipetted onto the surface of the disk B "puck" surface to ensure complete coverage. When the puck surface had been fully contacted, a photograph of the surface was taken to record the color changes.

2.4 Oxidation Front Measurements

Cr and ^{99}Tc are both redox sensitive contaminants present in the simulant and incorporated into the Cast Stone monoliths. The oxidized form of these contaminants (Cr(VI) and [99]Tc(VII)) is soluble and therefore more leachable, whereas the reduced form (Cr(III) and [99]Tc(IV)) is insoluble and is relatively less leachable. Thus the concentration of leachable Cr and ^{99}Tc in the monolith sections in a fast water leach test will give an indication of the extent of oxidation. A detailed description of this fast water leach test can be found in several reports (Almond et al. 2012, Langton et al. 2013a, Langton et al. 2013b). This previous work at SRNL by Langton et al. developed an approach to investigate the ingress of O_2 by placing thin sections from a cured monolith into a small volume of DIW to observe the release of species in a short period of time (~24 h) (Langton et al. 2013a). The theory behind the approach is that any redox species already in an oxidized state will be rapidly released from the monolith while species in a reduced state will not have sufficient time to oxidize and be released. The results of that work, where a sole face of the monolith was exposed to the atmosphere and the remaining monolith surface covered showed a clear front of oxygen ingress into the monoliths by observing the change in Cr released. In this work, we performed a similar approach with slight modifications. A comparison of how the monoliths are prepared in this method, vs. the previous Langton et al. (2013) method can be seen in Figure 2-2.
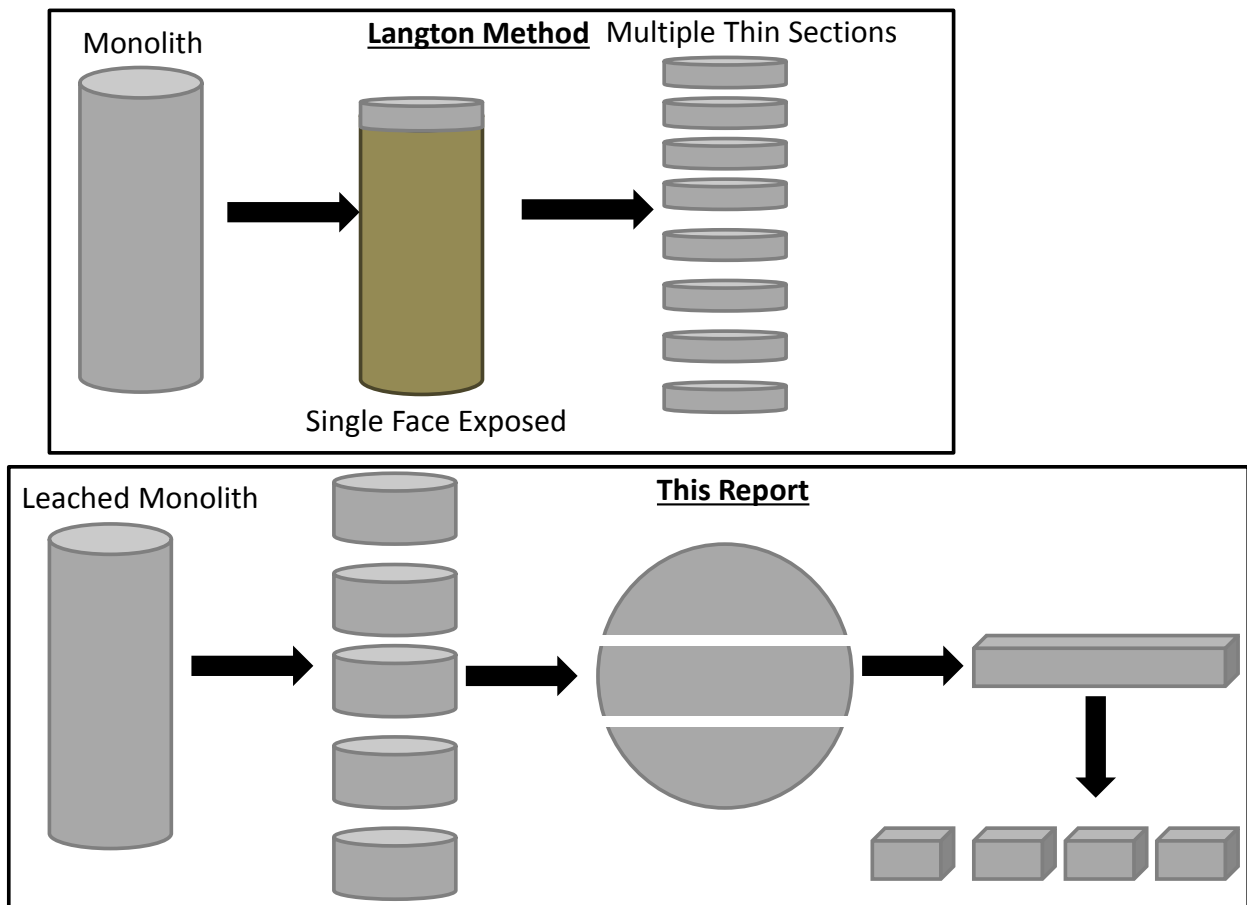
Figure 2-2 A comparison between the monolith preparations used in this report and in previous short term leach testing for oxidation front measurements.

The monoliths were sectioned into round pucks and a long rectangular piece was sectioned from the center of the disk (~0.5" or 13 mm thickness). The piece was removed from the anoxic chamber, further sectioned across the length of the piece and the dimensions measured with calipers. The individual pieces, representing difference distances from the monolith outer wall surface, were crushed to a < 300 µm particle size. An aliquot of each crushed piece (1 g) was then placed into a glass vial (20 mL) and

DIW water that had been de-aerated under a nitrogen flow for 4 h and continuously de-aerated during the experiment preparation, was pipetted into the vial. The volume of water added was determined the by mass of crushed Cast Stone in each vial. The vial was then capped, and parafilm was placed around the cap for an added barrier and returned to the anoxic chamber. This process took ≤ 20 minutes to complete from the initial removal from the anoxic chamber. The vials were then sealed into Mylar bags containing oxygen getters in the anoxic chamber, removed from the chamber and placed on a shaker for ~ 24 h.

Upon stopping the shaker, the vials were given 4 h to settle before the bag was opened. The solution was filtered with a 0.45 µm filter and the residual solids collected. The pH and E_h of the collected solution was recorded and the solution submitted for analysis by inductively coupled plasma- mass spectroscopy (ICP-MS) for Tc and inductively coupled plasma optical emission spectroscopy (ICP-OES) for Cr.

The residual solids were then weighed and placed into a 105 °C oven in a moisture content tin. After 24 h the sample was removed from the oven and weighed. This process was repeated until the recorded masses were within 0.05 g of the previous interval. The dried solids were then acid digested in 8 M Nitric Acid using ASTM-D5198-09 "Standard Practice for Nitric Acid Digestion of Solid Waste" (ASTM 2009) and the digestates were analyzed using ICP-MS for Tc and ICP-OES for Cr. Plastic tubes were used instead of glass beakers in the digestion step and samples were heated in an oven set at 95°C for 24 h to promote solids dissolution.

2.5   Solid State Characterization

2.5.1   X-ray Diffraction (XRD)

Monolith pieces were crushed to a < 300 µm particle size for analysis with X-ray diffraction (XRD). A known amount of rutile standard was added to each sample to facilitate semi-quantitative analysis. The crushed sample was placed in a mortar along with the rutile at a mass ratio of ~ 10:1 and further ground and mixed with a pestle prior to analysis. These powders were loaded into a zero-background holder and diffraction data were collected with a Rigaku Miniflex II Bragg-Brentano diffractometer using Cu-Kα radiation (λ = 1.5418 Å) and a graphite post-diffraction monochromator. Quantitative Rietveld refinements were carried out with the Bruker TOPAS software (v4.2, Bruker AXS) using crystal structures for the relevant phases. Error on amorphous fraction is ± 3% for the absolute value and for the crystalline phases is ± 10% to the relative measurement.

2.5.2   Nuclear Magnetic Resonance Spectroscopy (NMR)

^{23}Na Direct Polarization (DP) measurements were conducted on a 17.6 Tesla wide bore Bruker Avance III spectrometer, utilizing a 3.2 mm triple resonance probe operating in HX mode tuned to a ^{23}Na frequency of 198.44874 MHz. Spectra were acquired by collecting 14336 transients using calibrated ^{23}Na $\pi/20$ pulses of 0.35 µs, a 500 kHz sweep width, a spinning speed of approximately 18 kHz, and a 1.0 s recycle delay. Time domain free induction decays were apodized with exponential functions corresponding to 100 Hz of Lorentzian broadening prior to Fourier transformation. ^{23}Na resonances were referenced to 0.1 M NaCl(aq) at 0 ppm.

^{27}Al DP measurements were also conducted on a 17.6 Tesla wide bore Bruker Avance III spectrometer, utilizing a 3.2 mm triple resonance probe operating in HX mode tuned to a ^{27}Al frequency of 195.49002 MHz. Spectra were acquired by collecting 16384 transients using calibrated ^{27}Al $\pi/20$

pulses of 0.30 µs, a 500 kHz sweep width, a spinning speed of approximately 18 kHz, and a 1.0 s recycle delay. Time domain free induction decays were apodized with exponential functions corresponding to 150 Hz of Lorentzian broadening prior to Fourier transformation. [27]Al resonances were referenced to 0.1 M AlCl$_3$(aq) at 0 ppm.

The Cast Stone powders, < 300 µm, were solidified using Stycast© epoxy into a rod shaped form designed to fit the NMR probe.

2.5.3 Single Particle Digital Autoradiography

Single-particle digital autoradiography was used to measure the spatial distribution of ^{99}Tc and [238]U within Cast Stone cross sections (pucks) with the ionizing-radiation Quantum Imaging Detector (iQID) (Miller et al. 2015). The iQID imager comprises a scintillator in direct contact with a micro-channel plate image intensifier and a lens for imaging the intensifier screen onto a charge coupled device (CCD) or complementary metal oxide semiconductor (CMOS) camera sensor, all within a compact light-tight enclosure. iQID is sensitive to a broad range of radiation including gamma-/X-rays, neutrons, spontaneous fission, conversion electrons, alpha and beta particles. Individual photons or particles absorbed in a scintillator crystal or phosphor screen produce a flash of light that is amplified via the image intensifier by a factor of 10^4 to 10^6 and then imaged onto the camera. Scintillation flashes associated with individual events are finely sampled with an array of pixels and referred to as an event cluster. iQID's ability to localize charged particles, both spatially and temporally, on an event-by-event basis enables radionuclide distributions to be quantified at mBq -levels. Autoradiographs are constructed in real time at high spatial resolutions with an unrestricted dynamic range. The intrinsic spatial resolution of the detector has been measured to levels as high as 20 µm with alpha decays. iQID is a portable, laptop-operated system that requires no cooling and leverages the ever-increasing advances in CCD and CMOS camera sensor technology. For the imaging experiments, a 4-megapixel camera (2048 × 2048 pixels) was used that acquires full-resolution images at approximately 10 frames per second. Disks sectioned from within ~ 0.5" from the center of the monoliths were analyzed using the iQID. The disks had a smooth surface, were placed on a scintillation screen for collection times of 45 h. The effective physical size of each pixel during the image acquisition was 55.8 µm with the final images displayed having an effective pixel size of 111.5 µm (2x2 binning). The pixel value corresponds to the number of beta particles detected at that location during the 45 h image run. Further information on the development and use of the iQid technique can be found in a previous publication (Miller et al. 2015).

2.5.4 X-ray Absorption Spectroscopy (XAS)

Iodine K-edge X-ray absorption spectroscopy (XAS) data were obtained at the Stanford Synchrotron Radiation Lightsource Beamline 11-2, with the monochromator detuned by 50% to reduce the harmonic content of the beam. Transmission data were obtained using Ar filled ion chambers and fluorescence data were obtained using a 100 element Ge detector; the data were corrected for detector dead time. Data were converted from raw data to spectra using SixPack(Webb 2005). Spectra were normalized using Athena (Ravel et al. 2005). Samples were ground monolith powders, < 300 µm particle size.

2.5.5 Scanning Electron Microscopy (SEM)/X-ray Energy Dispersive Spectroscopy (EDS)

SEM examinations were carried out using an FEI Quanta250 Field Emission Gun equipped with a backscattered electron (BSE) detector and EDAX Genesis x-ray energy dispersive spectrometer (EDS) system. Elemental mapping and line-profiles were performed with the aid of drift-correction software. Semi-quantitative EDS results were obtained using standard ZAF correction conditions and are useful for comparative analysis not quantitative analysis, owning to the uneven surface, variable density and porosity of the materials examined. SEM images were obtained between 10 and 30 keV with both secondary and backscattered detectors to enable the features of interest to be observed most clearly. The SEM magnification scale was checked against a NIST traceable standard, MRS-4. The EDS energy scale was calibrated against the k-lines of a Cu-Al standard

2.5.6 Micro X-ray Fluorescence Spectroscopy (µ-XRF)

µ-XRF analysis was performed using an Orbis Micro-XRF Analyzer with a Mo tube (50kV, 50W). Elemental data were collected using a polychromatic beam focused to 30 µm using a poly-capillary optic and displayed as number of counts per energy.

2.5.7 Biological Characterization

Apparent biological growths were observed on the monolith surfaces of most of the Cast Stone monoliths leached in VZPW, and previous work has suggested biological activity being responsible for upticks in the nitrite content of the VZPW eluates (Serne et al, 2016). Confirmation of the identity of the microorganism was attempted as follows. The growths were scraped from the surface of a monolith (T18LCS2-7.8RAS-3, leached in VZPW from Serne et al. 2016) immediately after removal from solution and placed into a phosphate buffered saline solution. The T18LCS2-7.8RAS-3 monolith was returned to its archived solution afterward and care was taken to not disturb the outer layer on the monolith. Samples of the growths were initially stained with DAPI (4,6-diaminophenylindole), which is a fluorescent stain that binds to DNA in cells. These analyses showed the presence of bacteria in the samples. Following identification of microbes in these samples DNA was extracted from the samples using a MoBio Powersoil DNA Isolation Kit, and quantified using a NanoDrop spectrophotometer. DNA barcodes and linkers were added using polymerase chain reaction and the resulting amplicons were sequenced at the Institute for Genomics and Systems Biology Next Generation Sequencing Core Facility at Argonne National Laboratory using an Illumina MiSeq instrument. Demultiplexing, quality filtering, and operational taxonomic unit picking were performed using the Quantitative Insights Into Microbial Ecology toolkit v. 1.8.0) (Caporaso et al. 2010, Kuczynski et al. 2012). Raw sequence material was processed in silico, and taxonomy was assigned to operational taxonomic units using BLAST alignments compared to the SILVA ribosomal RNA gene database project.

3.0 Results

3.1 Removal of Cast Stone Monoliths

Six long-term leached Cast Stone monoliths were removed from their final leachant storage solution (see Table 2-1 for details), which was an aliquot of their final leachate, to perform solid state characterization. Upon removing the monoliths from the leachate, an initial inspection of their features was made, prior to detailed characterization. Figure 3-1 shows the monoliths immediately after being removed from solution. T5-VZ (Figure 3-1 a), which was leached in VZPW has the common white particulate layer formed on its outer surface. Previous characterization of the white precipitate (Serne et al. 2015, 2016) determined that it was predominately aragonite, a polymorph of calcium carbonate. T5-DI (Figure 3-1 b) was from the same Cast Stone fabrication batch but leached in deionized water (DIW) and had no white precipitate, although several surface cracks were visible that were infilled with white precipitate. The aragonite film was again present on the T10 monolith leached in VZPW (Figure 3-1 c). The T17 monolith (Figure 3-1 d) shows an incomplete white deposit on its surface after leaching in DIW. The film on T17 was not characterized, but is likely aragonite with ingress of CO_2 from the atmosphere supplying the CO_3. T14 also had a visible aragonite film after leaching in DIW (Figure 3-1 e) and several dark spots were present on its outer surface, similar to the features present on T17 (Figure 3-1 f). The T5-DI and T5-VZ monoliths were leached for 569 days before being stored in their respective final leachates for 393 days, the T10 and T17 monoliths were leached for 590 days and then stored in their final leachates for 392 days, the T14 monolith was leached for 590 days before being placed in its final leachate for 383 days and the T21 monolith was leached for 590 days before being placed in its final leachate for 319 days. After removal from their respective final leachates, the monoliths were inspected visually (i.e. photographed) and characterized in detail.
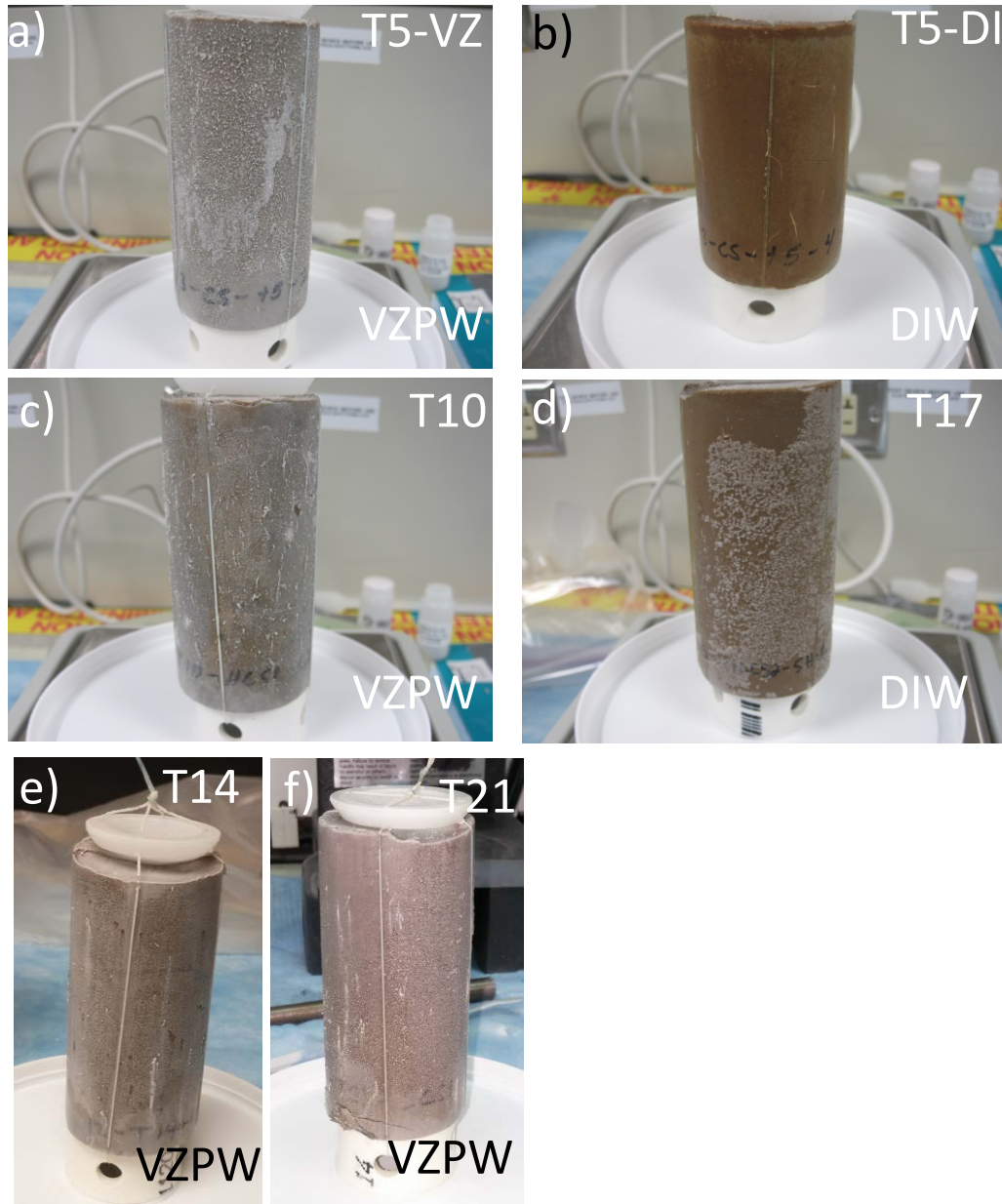
Figure 3-1 – Photographs of the six monoliths selected for this study immediately following their removal from the archived solutions.

3.2 Carbonation Ingress

Throughout leaching of Cast Stone monoliths following EPA Method 1315, a multitude of chemical aqueous species are capable of moving both into, and out of, the monolith. The potential exists for these processes to alter the solid state characteristics of the Cast Stone. One such species is CO_3^{2-}, which can lower the alkaline pH within the monolith by reacting with calcium-bearing phases present in the Cast Stone to form calcium carbonate (Zha et al. 2016). CO_3^{2-} is a component of the VZPW (added as $NaHCO_3$) and is also present in DIW as dissolved CO_2 from the atmosphere but at lower concentrations. There is carbonate already present in the LAW simulant and may be still be present in the monolith. This

method looks at the movement of additional CO_3 into the monolith from external sources and working with the initial CO_3 inventory to alter the pH of the grout. To investigate carbonation ingress, phenolphthalein staining was used to show any changes in pH as a function of distance from the monolith surface. The T5-DI, T5-VZ, T10 and T17 monoliths were sectioned into disks inside a glove box under a N_2/H_2 atmosphere and cleaned with a brush to remove any dust from the dry diamond saw cutting. Phenolphthalein was added to the freshly exposed bottom face of section B from each monolith (Figure 2-1) inside the anoxic chamber. The resulting surfaces are shown in Figure 3-2.

b) T5-DI
1 cm
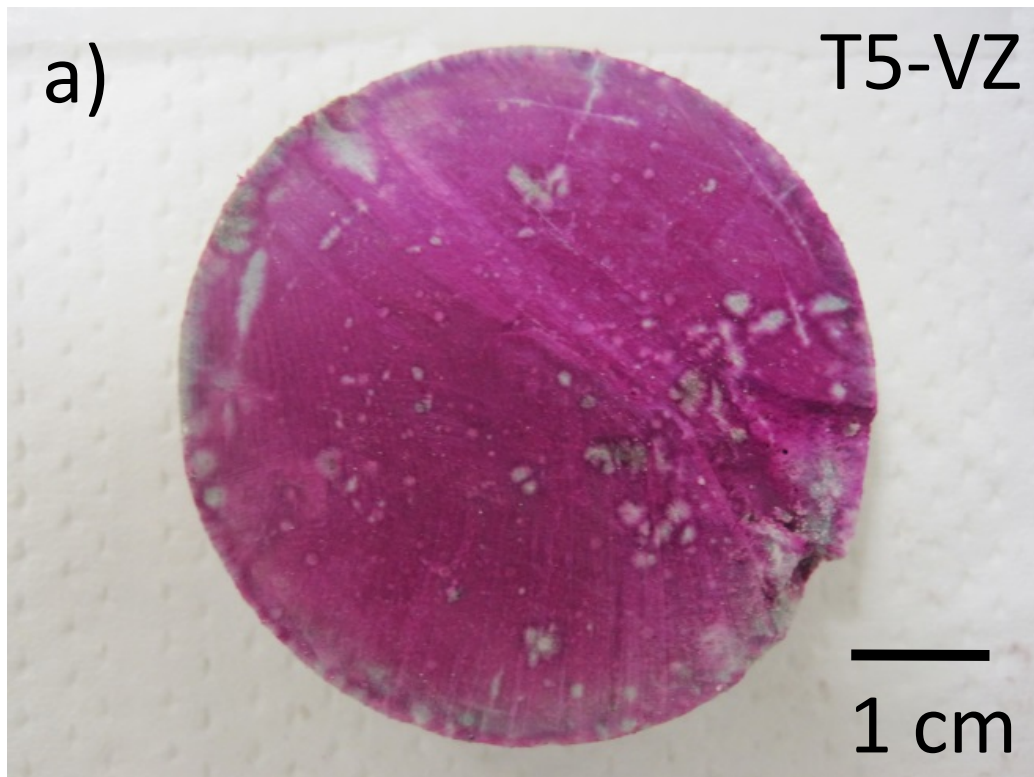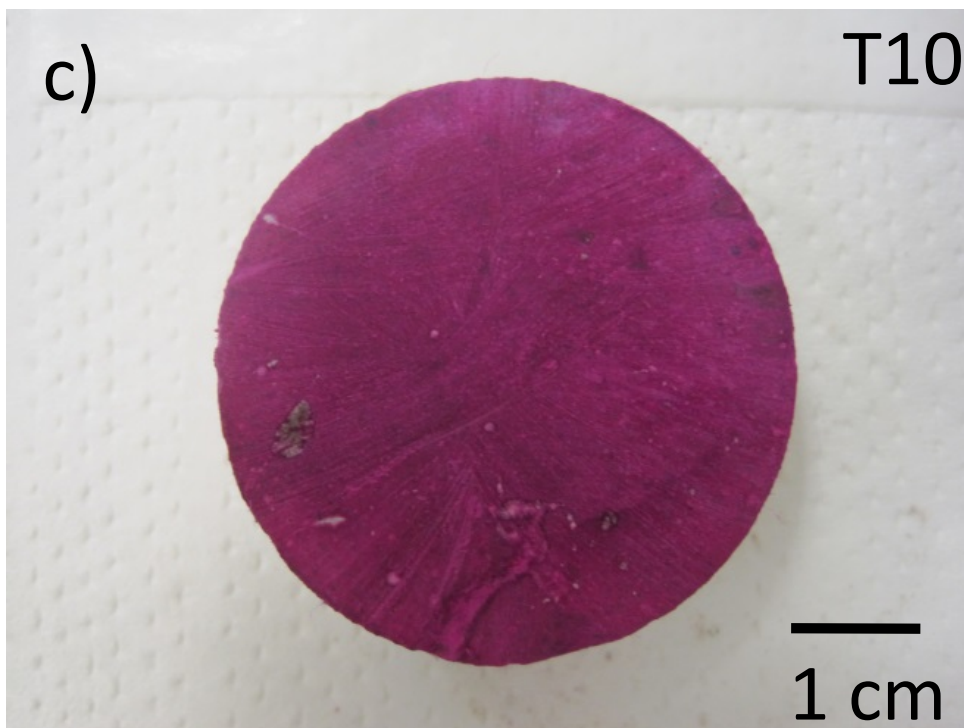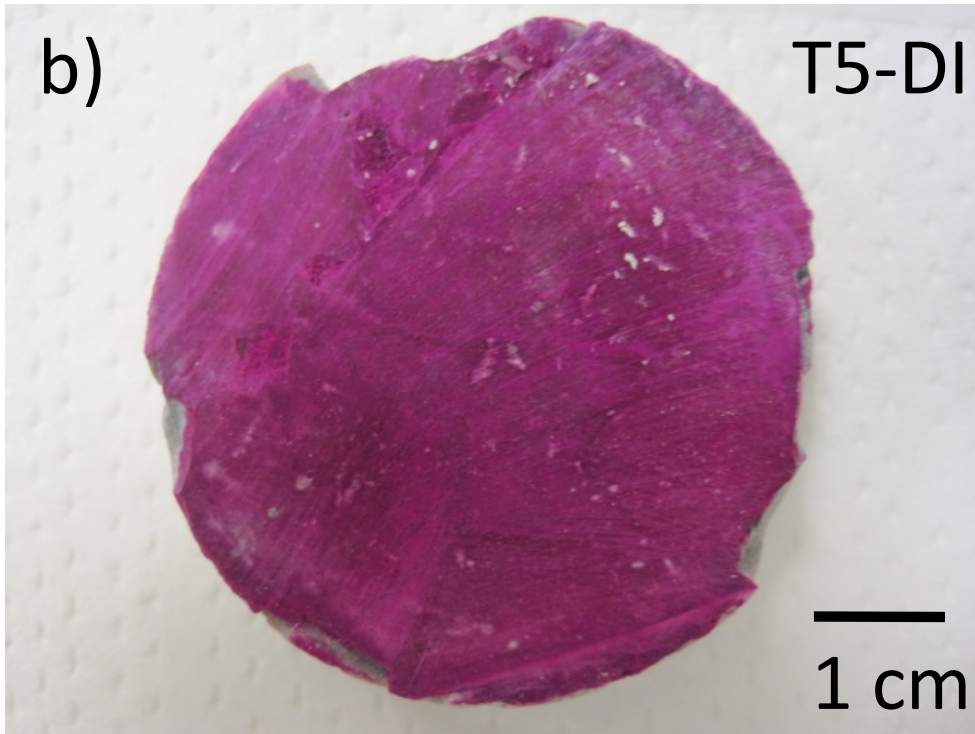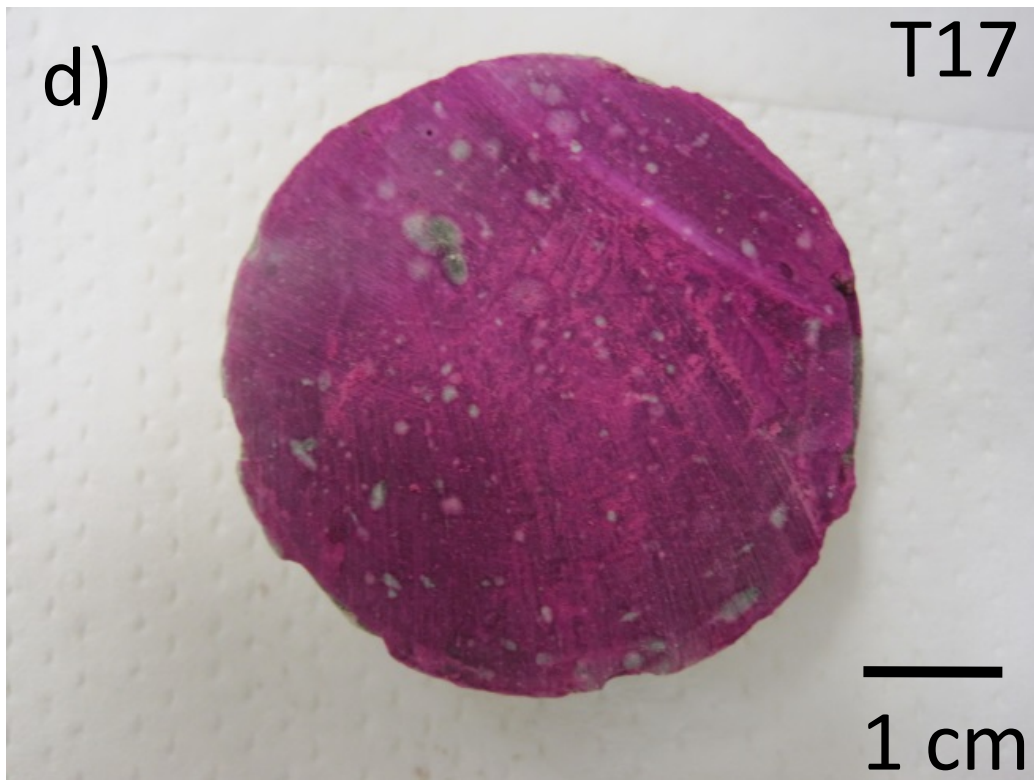
c) T10
1 cm

Figure 3-2 – Photographs following the phenolphthalein staining of the a) T5-DI, b) T5-VZ, c) T10 and d) T17 monoliths in the anoxic chamber. The presence of the deep pink/purple color indicates a pH $\geq$ 9.8.

From the images, there was no visible carbonation front on any of the monoliths as the phenolphthalein remains dark pink, indicative of pH $\geq$ 9.8, over the entire surface. The T5-VZ monolith (Figure 3-2 a) had some areas that did not change color near the edge, but the phenolphthalein staining was complete all the way to the edge for the majority of the monolith. This may be evidence of initial CO_3^{2-} ingress, between 20 mm to 40 mm in the top left corner of the image but no other CO_3^{2-} ingress along the rest of the outer wall circumference was evident. Some colorless areas were visible in the interior of the monolith, possibly suggesting some pockets of lower alkalinity. The T5-DI monolith (Figure 3-2 b) also had some colorless areas but again the dark pink/purple staining was complete to the outer edges. The T10 monolith surface (Figure 3-2 c) showed the most complete surface dark pink/purple staining. The T17 monolith (Figure 3-2 d) also had several small colorless areas, but no evidence for an outer colorless rim around the edge of the disk.

The indicator test is likely to underestimate carbonation as a color change would occur even if the pH is less alkaline than the initial Cast Stone pH, but the results in Figure 3-2 suggest that no significant CO_3^{2-} ingress occurred during the extended leaching of the Cast Stone monoliths. However, investigation of the T21 monolith showed that upon removal from its final leachate, signs of rubblization were observed with a significant piece easily removed from the bottom of the monolith (Figure 3-3 a). At the interface between the spalled piece and the bulk monolith a white deposit was observed. When cracking the monolith, the outer portion of the monolith (~ 55 mm) easily broke away and, at the interface of this region and the bulk monolith, a white deposit was again observed (see red arrow in Figure 3-3 b). As the T21 monolith was leached in VZPW with the calcite/aragonite film present on the outer wall of the

monolith, this internal deposit may be further carbonate ingress from the outer wall. When phenolphthalein was placed on the outer wall of the T21 monolith in an area where the calcite/aragonite film was scraped away, the outer wall of the monolith appeared pink and darker on the interior (Figure 3-3 c). The staining came to an immediate stop when it contacted the remaining white film (red arrow in Fig 3-3 c). This shows that even the outermost surface of the monolith still retained its alkaline nature. The cross section of the T21 monolith outer wall (Figure 3-3 d) showed pores filled with a white deposit at the same approximate depth as the white deposits seen in Figure 3-3 b). Application of phenolphthalein to this surface showed staining complete to the monolith wall; however, the white pores did not change in color, which indicates carbonate neutralization in this localized area.
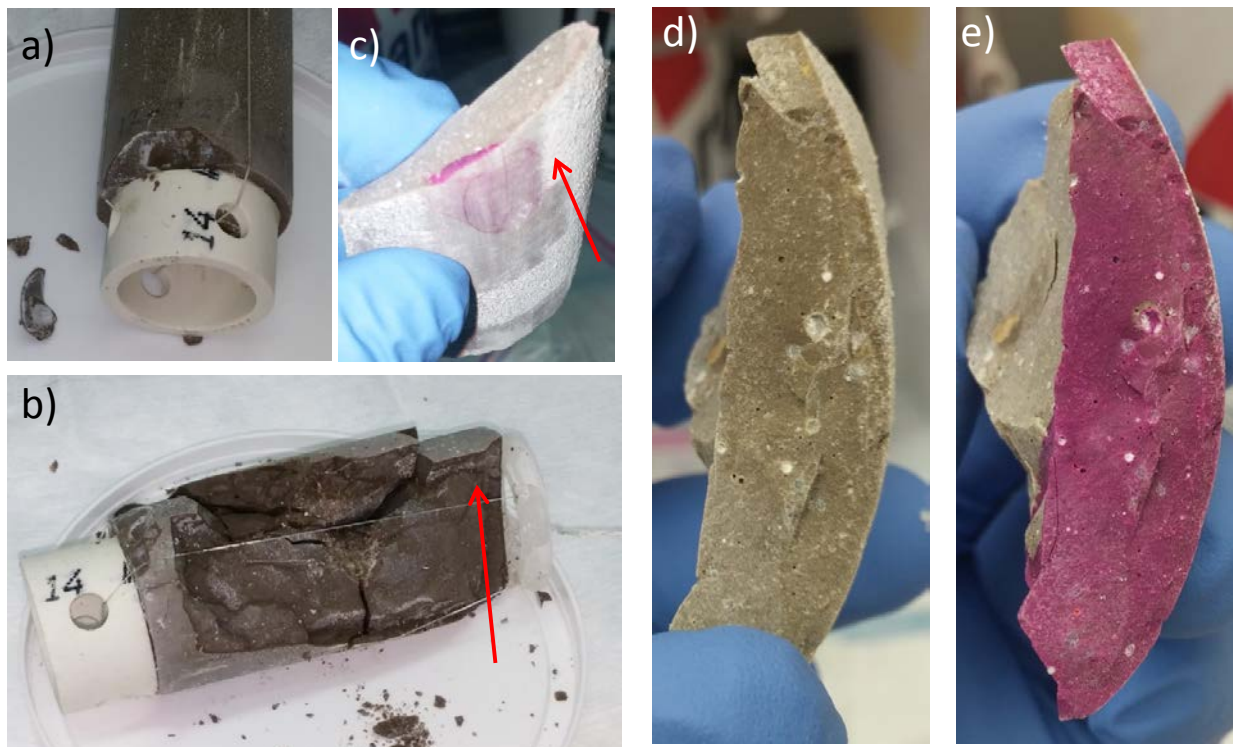
Figure 3-3 – Photographs of the T21 monolith showing a) spalling of a piece from the bottom of the monolith and appearance of the white precipitate, b) the "outer skin" revealed upon manual cracking, c) phenolphthalein staining of the outer wall of T21, d) a section of the outer wall of the monolith showing pores filled with a white deposit and e) the same surface after staining with phenolphthalein.

A filled pore from this region was extracted and analyzed with SEM/EDS (Figure 3-4). The large pore is partially filled with needle-like deposits, and a smaller filled pore can also be seen in the image (Figure 3-4a). A micrograph of the pore contents at higher magnification confirms a needle-like structure (Figure 3-4 b). An EDS line scan moving from within the pore out to the monolith along the arrow in Figure 3-4 a) was performed and the resulting elemental compositions are shown in Figure 3-4 c). Ca, S and Al were present in the pore, but S decreased significantly out of the pore with a concurrent increase in Si. These white deposits from the pore and inner wall of the monolith were collected and analyzed with XRD. A semi-quantitative fit showed the deposit to be ~ 60% ettringite, ~15 % brucite, ~ 10% calcite, ~10 % aragonite and ~ 1% hydrocalumite, < 1% hemicarbonate and quartz. The needle-like morphology suggests that the mineral phase is ettringite $Ca_6Al_2(SO_4)_3(OH)_{12} \cdot 26(H_2O)$ (Stutzman 2001).
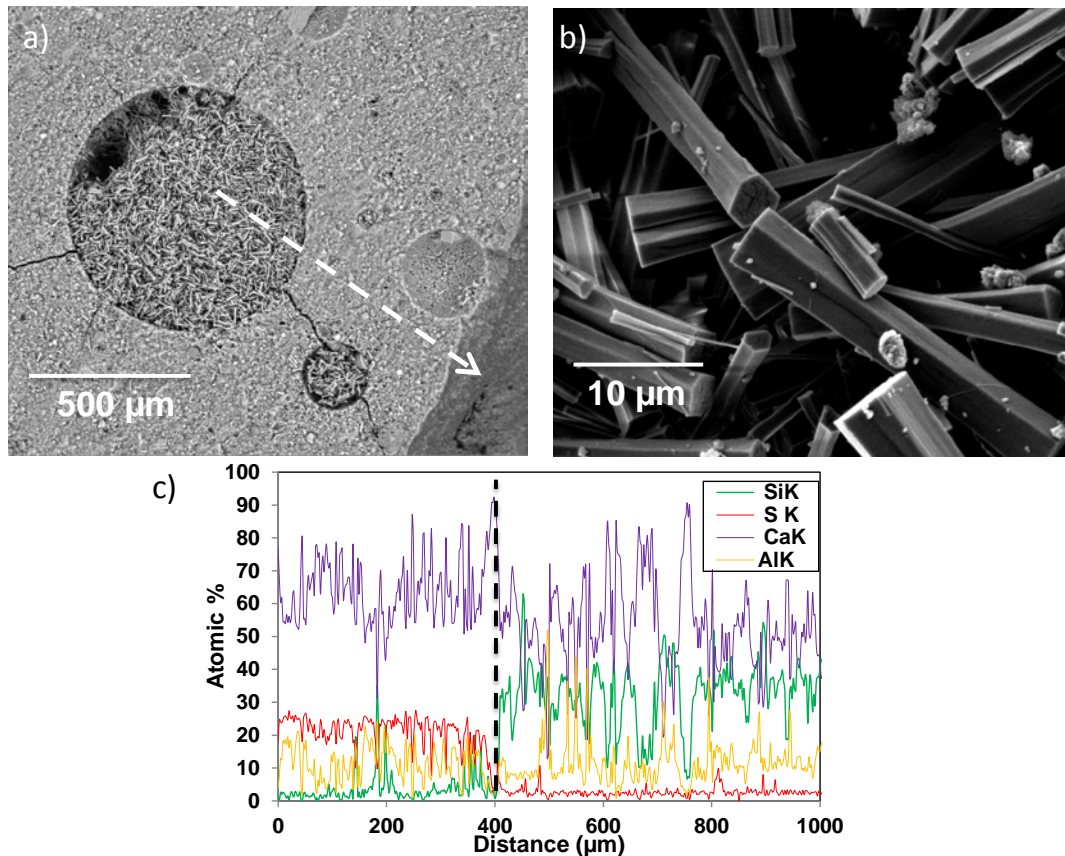
Figure 3-4 – a) SEM image of a pore from the T21 monolith filled with the white deposit, b) SEM image of the contents of the pore, c) elemental results from the EDS line scan moving along the dotted arrow in a). The dotted black line in C shows the point of transition from the pore to the bulk monolith in the line scan.

The timing and mechanism of ettringite formation within these pores is currently unclear, however no sign of ettringite was observed in XRD analysis of bulk pieces of the extended leached Cast Stone monoliths, nor in un-leached monoliths fabricated in FY16 (see Asmussen et al. 2016). During leaching, the VZPW will enter the monolith via its pores/surface micro-cracks and this will change the internal Cast Stone pore liquid composition, which could promote aragonite formation. This change in internal Cast Stone pore liquid , in combination with monolith dissolution over time releasing Al, could result in the deposition of secondary minerals, such as ettringite. Formation of ettringite via this mechanism after the monolith has set (hardened) would result in volume expansion, which could lead to rubblization. This may have caused the easy removal of the outer ~5 mm "skin" on the T21 monolith. These initial observations are not conclusive and a comprehensive investigation of archived long-term leached monoliths is required to establish the onset of secondary mineral formation and extent of the ingress of these secondary minerals into the monoliths.

The amount of CO_3^{2-} entering the monolith via the VZPW is not large enough to overcome the alkaline nature of the bulk monolith's surface, based on the phenolphthalein staining. However, within individual pores, carbonation occurred as evidenced by the presence of small amounts of calcium carbonate (20%) along with higher amounts of ettringite (60 % from XRD), and other mineral transformations were induced as evidenced by the presence of significant amounts of ettringite. These deposits extended ~ 5 mm into the monolith after several years of leaching.

3.3 Oxygen Ingress

During curing, the Cast Stone monoliths are a reducing environment due to the alkalinity and redox active components such as BFS. Over time oxygen from the atmosphere and dissolved in the leaching solution can penetrate into the monolith and the oxidation of redox sensitive contaminants (such as Tc and Cr) can occur and eventually overcome the reducing environment of the grout. Initial Tc and Cr oxidation states are assumed to be uniformly distributed throughout the monolith based on the assumption that the BFS is homogeneously distributed in the cured solid. Not all Tc is expected to be in the reduced Tc(IV) form within the monolith after curing for several months based on XANES measurements (see (Um et al. 2013, Asmussen et al. 2016)). The incomplete reduction of TcO_4^- present from the liquid waste simulants has been interpreted as slow reaction of the reductant BFS solids with the Cast Stone internal pore fluids (comprised of Hanford liquid waste simulants). Further, as BFS-containing grouts continue to cure and be stored in containers, typically plastic bags containing moist paper towels, movement of oxygen, permeating through bags, inward to the monolith can assist in re-oxidation of Tc(IV). These processes may lead to enhanced release of Tc and Cr as their oxidized states (i.e. Tc(VII) and Cr(VI)) are more soluble than their reduced forms. An attempt to quantify oxygen ingress relative to the monolith outer wall was made using short-term DIW leach testing of selectively sectioned monolith pieces (see Langton et al. 2013 for more details). Monoliths were sectioned in an anoxic chamber and the sectioned pieces were taken from the central disk (Section C in Figure 2-1) with three pieces taken from the disk moving from the wall (piece 1) to the center (piece 3), respectively in Figure 2.1. Prior to removal from their archive leaching solution, the monoliths had exposure to the open atmosphere while leaching in a saturated water environment, while sampling the monoliths were exposed to open air for ~2 min each sampling over the three year leaching period and a final, short exposure (< 2 min) when removed from their archive leaching solution.

The percentage of the species of interest leached was determined using the following equation:

$$\% \text{ Leached} = 100 * \left(\frac{m_{i-\text{leachate}}}{m_{i-\text{total in solid}}} \right)$$

Equation 3.1

Where:
$m_{i-\text{leachate}}$ = mass of species i leached (mg) into the DDI.
$m_{i-\text{total}}$ = mass of species i in the residual solids plus the mass of the species in the water leachate (mg). This is the total inventory of the species.

The aim of these short-term DIW measurements was to determine significant differences in % leached values as a function of distance from the outer edge of the original monoliths. The distance at which the significant change in % leached occurs represents an indirect measure of oxygen ingress. The monoliths were assumed to have a homogenous distribution of Tc and Cr in these calculations, although Section 3.4.4 shows that this may not be the case.

For all short-term DIW leachates, the pH ranged between 11.6 and 12.1 and the E_h ranged from -47.3 mV to -63.2 mV and the pieces of Cast Stone monoliths subjected to the short-term leaching had a gravimetric moisture content ranging from 23 - 26%. Figure 3-5 a) shows the % Tc released in the three sections for the T5-DI, T5-VZ, T10 and T17 monoliths. The mean distance relative to the outer wall was used to average the distance of the selected pieces. All measurements are the average of duplicate leached aliquots . A general increase in %Tc released toward the inner portion of the monolith was observed for both the T5-DI and T5-VZ monoliths. At an average depth of 4.8 mm, T5-DI released 10.5 % of the total

Tc while at 23.7 mm 28.1 % of the Tc was released. Compared with the T5-VZ monolith where at 6.9 mm 22.6 % of the Tc was released and at 23.0 mm, 33.1 % of the Tc was released. The T10 monolith measured 13.7 % of the total Tc released at a distance of 2.2 mm from the wall and 18.6 % at 23.6 mm depth. T17 continued this trend by releasing 19.3 % of the Tc at 3.5 mm from the wall and 24.2 % at 24.5 mm from the outer wall.

The release of Cr from the same samples is shown in Figure 3-6 b). Here the outer sections again have the lowest %Cr release compared with the inner sections. The T5-DI released 0.29 % of the total Cr at 4.8 mm and 0.57% at 23.7 mm. The T5-VZ released 0.74 % at 6.9 mm and 0.94% at 23.0 mm. The T10 samples released 0.12 % of the Cr at 2.2 mm and 0.24% at 23.7 mm. The T17 samples released 0.14 % of the initial Cr at 3.5 mm and 0.31 % at 22.5 mm.
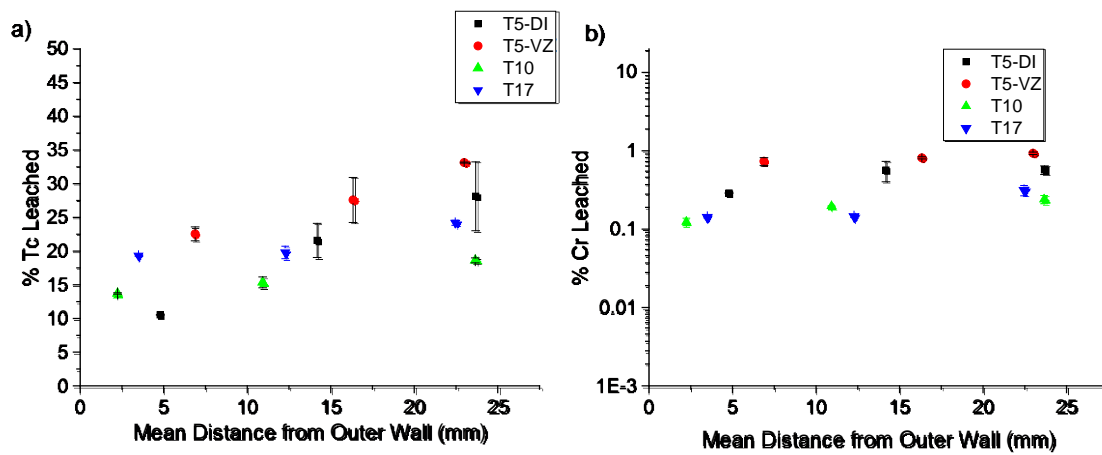
Figure 3-5 – plots of a) % Tc leached and b) % Cr leached from the short term leach tests to monitor oxygen ingress for the T5-DI, T5-VZ, T10 and T17 monoliths. The mean distance of the monolith section was used as a location. The error bars are the standard deviation of the mean for duplicate runs. Due to the level of change in % Cr leached b) the plot is shown as a logarithmic scale.

The expected trend of limited oxygen ingress would be a higher % of redox sensitive species release from sections near the outer wall. However, this was not the case in this measurement of the long-term leached Cast Stone monoliths. In the Langton and Almond (2013) and Langton et al. (2013) work, with a single face of the monolith exposed to partially water saturated conditions, oxygen ingress was found to increase release of Tc (~40%) and Cr(~ 5%) near to the exposed face. In our tests following the monoliths' exposure to water saturated conditions in the open atmosphere for several years, these trends are not observed. For Tc in our monoliths completely submerged on all sides for several years, between 15-30% of the Tc was leached, and values below 20% were considered "unaltered" in the Langton tests (Langton and Almond 2013). For Cr < 1% was leached in our monoliths, again a value considered to be from an "unaltered" region in the development of the technique (Langton et al. 2013). Due to this, it is unlikely oxygen has had much ingress into the monoliths following the several years exposure to the saturated conditions in our extended leach tests. Therefore, the Tc and Cr releases observed are likely controlled by other factors including:

(i)   species distribution (see section 3.4.4) where Tc may congregate near the outer wall or in discrete hot spots. We also speculate that Cr distributions in the leached monoliths might be similar to the inhomogeneous Tc distributions;

(ii)   inherent reductive capacity of the waste forms where the BFS can control Tc and Cr re-oxidation and subsequent release;

(iii)   available pathways out the monolith being lowered as the pores fill with precipitates such as ettringite and calcium carbonate.

Excessive oxygen ingress may eventually overcome reducing conditions in the monolith, altering the speciation of redox active contaminants. Under oxidizing conditions, iodide may be oxidized to iodate as well. For this reason, XANES spectra were collected on the T21 monolith, calculated to have the highest inventory of I in all the monoliths leached in the long-term tests performed by Serne et al. (2016). The iodine K-edge XANES spectrum for T21 is shown in Fig. 3-6. Due to shorter core–hole lifetimes during X-ray absorption processes for higher atomic number elements, such as iodine, XANES features are broadened. However, iodine K-edge XANES for iodate phases have an edge peak near 33,176 eV, whereas the more reduced iodides have nearly featureless edges with weak oscillation amplitudes above the edge (McKeown et al. 2015). Thus, the iodine K-edge XANES spectrum for T21 is most similar to that for the iodide, with the edge near 33,184 eV. Thus after a few years of leaching under open atmosphere conditions iodine speciation inside the Cast Stone remains iodide, which is the species present in the LAW waste simulant. This supports the findings in the short-term DIW leach tests, which suggested the little O_2 ingress had occurred in the long-term leached Cast Stone monoliths subjected to continual EPA-1315 leach testing. An example of I-speciation spectra for iodide (I^{1-}), iodate (I^{5+}) and iodine (I^0) standards can be found in a separate publication(Kodama et al. 2006).
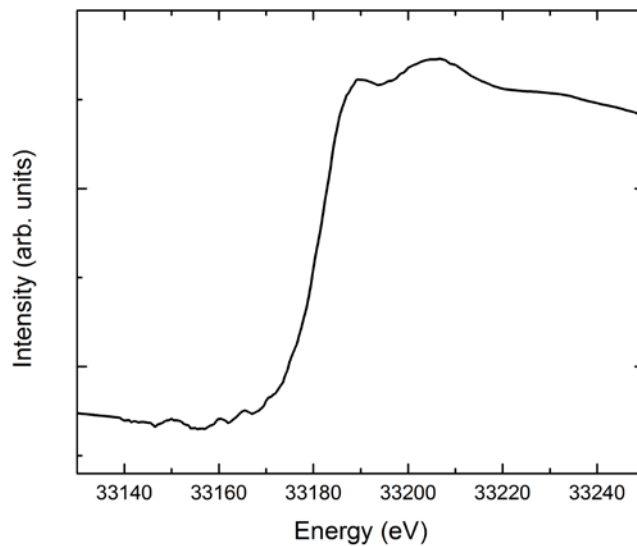
Figure 3-6 – The iodine K-edge XANES spectrum collected from the T21 monolith.

3.4   Solid State Characterizations

3.4.1   X-Ray Diffraction

XRD patterns as a function of 2θ based on $Cu_{K\alpha}$ radiation (λ=1.5418 Å) were measured for samples from the interior and exterior of the long-term leached Cast Stone monoliths to identify the mineral phases present and to quantify the amorphous component as a function of distance from monolith surface. The crystalline solid phases identified by XRD as being present in the monoliths, including relative amounts, are summarized in Table 3.1. Although there are errors associated with quantitative XRD measurement of these challenging, predominantly amorphous samples, analyzing multiple samples

in the same way to look for trends in the data provides useful information. The calculated and observed background-subtracted XRD pattern for the sample from the inside of monolith T21 is shown in Figure 3.7, along with the fits from Rietveld refinement for the respective mineral phases present, including the rutile standard. Although TiO_2 is present in the BFS, it constitutes <1wt.% (Westsik et al. 2016) and there is no evidence for rutile in the XRD patterns for samples measured without the added rutile standard, therefore the small amount of TiO_2 in the BFS will not impact on the quantitative XRD results reported.

Table 3-1 – Quantitative XRD measurement for the monoliths from this study. Rutile TiO_2 was added as a known standard in the measurement. Error for the measurements is assumed at ~10% of the reported value.

Sample	Hydrocalumite	Hemicarbonate	Hydrotalcite	Calcite	Tobermorite	Brucite	Sodalite	Cancrinite	Quartz	Mullite	Amorphous
Inner T14	0.5%		2.8%	1.1%	8.9%		2.0%		1.5%	4.0%	80%
Outer T14	0.6%		2.9%	3.7%	8.7%	1.2%	1.2%	0.7%	1.8%	4.7%	77%
Inner T21	0.4%		1.1%	5.0%	9.7%		5.8%		2.0%	4.1%	72%
Outer T21	0.1%		1.2%	5.7%	6.9%	2.8%	4.5%	2.0%	3.2%	5.2%	68%
Inner T5-DI	1.3%		3.3%	2.9%	16%		0.8%	8.4%	2.5%		65%
Outer T5-DI	1.1%		3.6%	3.4%	12%			7.1%	1.0%		71%
Inner T5-VZ	1.2%		3.5%	3.0%	25%			10%	1.5%		56%
Outer T5-VZ	0.1%		3.9%	3.9%	6.3%				1.7%	4.1%	80%
Inner T10	0.6%	1.0%	1.3%	3.9%	6.2%				1.5%		85%
Outer T10		0.4%	0.8%	4.4%	4.7%	1.1%			2.9%		86%
Inner T17	0.2%		3.3%	3.2%	6.2%				1.5%	3.9%	82%
Outer T17	1.1%		3.7%	4.4%	14%	3.1%		4.5%	2.0%		68%

All monoliths are dominated by the amorphous component (56-86% of the sample) with no evidence of variation as a function of distance from the monoliths' outer surface. In terms of crystalline phases, all monolith contain tobermorite $Ca_5Si_6O_{16}(OH)_2 \cdot 4H_2O$ (4.7-25%), calcite $CaCO_3$ (1.1-5.7%) and quartz SiO_2 (1.0-3.2%). A small peak present in all samples at low angle could be fit with varying amounts of the related hexagonal phases hydrocalumite $Ca_2Al(OH)_{6.5}Cl_{0.5} \cdot 3H_2O$, hemicarbonate $C_3A \cdot 0.5CaCO_3 \cdot 12H_2O$ and hydrotalcite $Mg_6Al_2(CO_3)(OH)_{16} \bullet 4(H_2O)$ (0.4-2.5%) with the angle of the peak position increasing depending on the phase (hydrocalumite < hemicarbonate < hydrotalcite). Poorly crystalline hydrotalcite, a hydrated magnesium silicate phase characteristic of hydrated slag systems, dominates in all samples (Serne and Westsik Jr2011). Quartz, hydrotalcite and hydrocalumite are evenly distributed throughout the monoliths. Calcite is present in higher amounts at the surface as compared to the interior of all the monoliths suggesting the ingress of CO_3 from both the VZPW and the DIW, and also from the initial CO_3 inventory of the LAW simulant. Tobermorite is predominantly present in higher amounts in the monoliths' interior. Sodalite ($Na_8(Al_6Si_6O_{24})Cl_2$) is present in the T14 and T21, with a small amount in one T5-DI sample. It is present in higher amounts in the monolith interior and the amount present increases with water to dry blend solids ratio (1.2-2.0 % in T14 and 4.5-5.8 % in T21). The T14 and T21 monoliths contain high concentrations of SO_4^{2-} and this has been shown to increase the rate of transformation from poorly crystalline aluminosilicate to sodalite in concentrated NaOH solutions. (Deng et al. 2006) The decrease in the amount of sodalite and the presence of cancrinite $Na_6Ca_2Al_6Si_6O_{24}(CO_3)_2$ at the surface of the T14 and T21 monoliths suggests that the sodalite converted to cancrinite at the surface. Cancrinite was also present in relatively high amounts in the T5 and T17 monoliths, especially in pieces representing the outer surface. Mullite $Al_{4.5}Si_{1.5}O_{9.75}$, a silicate mineral of post-clay genesis produced during various melting and firing processes, is present in T14, T21, T5 and T17 as these samples were fabricated using a lower Ca content Class F FA from the southeast of the USA, known to contain mullite crystalline phases. . XRD analysis of comparable monoliths before

leaching, described in a concurrent report (Asmussen et al. 2016) has shown that the monoliths transform over time resulting in an increase in the crystalline component and the transformation of mineral phases that are less thermodynamically stable, e.g. hemicarbonate and larnite, into more stable mineral phases, e.g. sodalite and cancrinite. Hemicarbonate ($C_3A \cdot 0.5CaCO_3 \cdot 12H_2O$), which forms due to the slow reaction kinetics of $CaCO_3$ at high pH, is still present small amounts in T10 and this sample also has the highest amorphous component, demonstrating that the rate of transformation is influenced by the type of liquid waste simulant that is being solidified. Brucite $Mg(OH)_2$ is present on the outside of all of the monoliths except the T5 set.
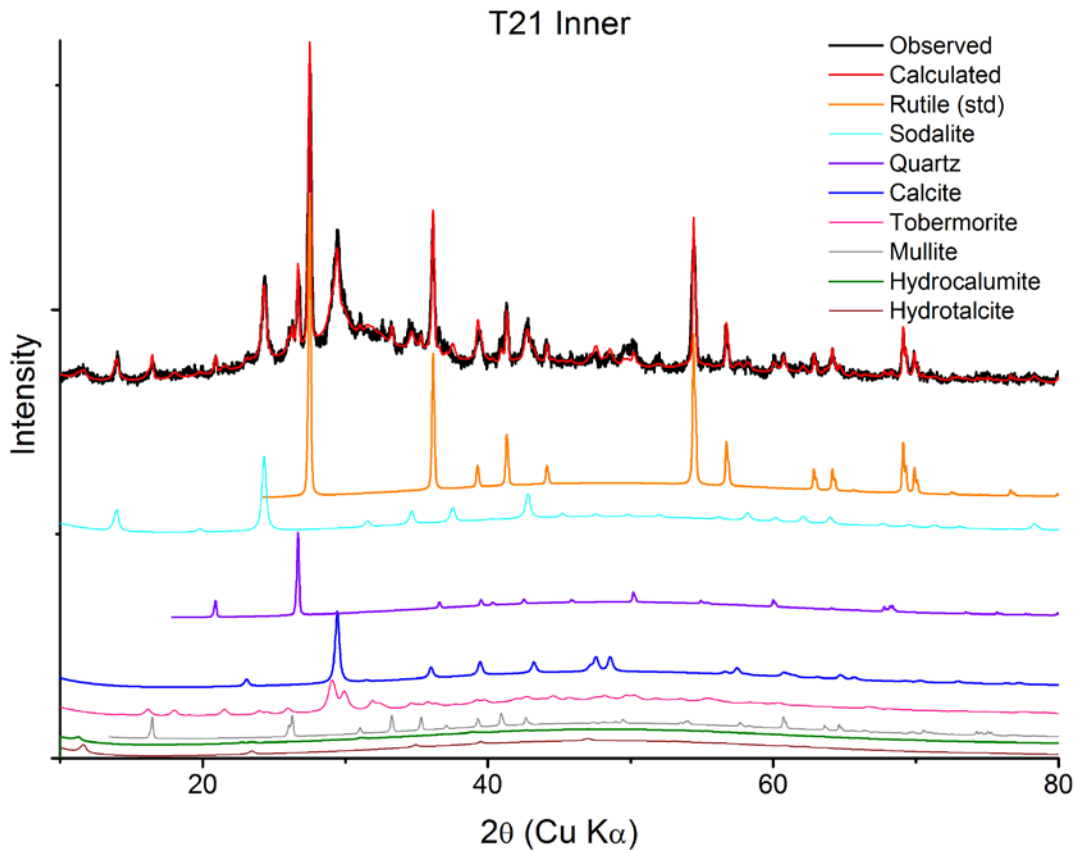
Figure 3-7 - Example XRD spectrum (black) and the spectra used for fitting and calculation of quantitative values for the T21 sample taken from the inner core of the monolith.

3.4.2   Nuclear Magnetic Resonance Spectroscopy (NMR)

The T21 and T14 monoliths were analyzed with ^{27}Al and ^{23}Na DP NMR to characterize any local bonding changes in the Cast Stone relative to the position in the monolith. Samples were taken from within 5 mm of the outer wall of the monolith (called OUT), and the central portion of the monolith ~25 mm depth from the wall (called IN). The samples were crushed to < 300 µm particle size and mounted as a cylindrical rod-like pellet in StyCast resin. For comparison, the spectra from an un-leached monolith

(T7) prepared with LAW simulant and the 47/45/8 BFS/FA/OPC mix from FY16 (T7 in Asmussen et al. 2016) is included.

The ^{27}Al spectra are shown in Figure 3-8. The un-leached T7 has two distinguishable ^{27}Al resonances in the tetrahedral region at ~ 75 and 62 ppm, and one in the octahedral region at ~10 ppm. Although long-term leached T21 and T14, both inner and outer pieces, exhibit ^{27}Al resonances at 75 and 10 ppm, the intensity is significantly reduced compared to the un-leached T7. Similarity is most evident in the intensity of the resonance at ~ 62 ppm, which is the dominant species in the T14 and T21 samples.

The T-21 samples contain similar tetrahedral Al species, but vary in octahedral Al, with T-21 Out containing two additional octahedral Al resonances, at 15 ppm and 0 ppm. The 15 ppm resonance also appears in the T-14 Out spectra, while all other spectra show the 0 ppm resonance at lesser intensity. Similar to T-21, T-14 samples exhibit the same Al patterns in the tetrahedral region, with variation occurring in the octahedral region, such as the resonance at 35 ppm. In addition, the proportion of octahedral Al in T-14 Out is significantly greater than any other sample. It is clear from these data that the Al phases present in the leached T-14 and T-21 monoliths vary with location in the monolith, where formation of octahedral Al phases occurs to a greater extent in the skin (Out samples) as compared to the inner core. This may be attributed to the effects on monolith composition of: (i) water diffusion (e.g. hydration state); (ii) monolith dissolution over time; and (iii) the availability of charge-balancing cations.
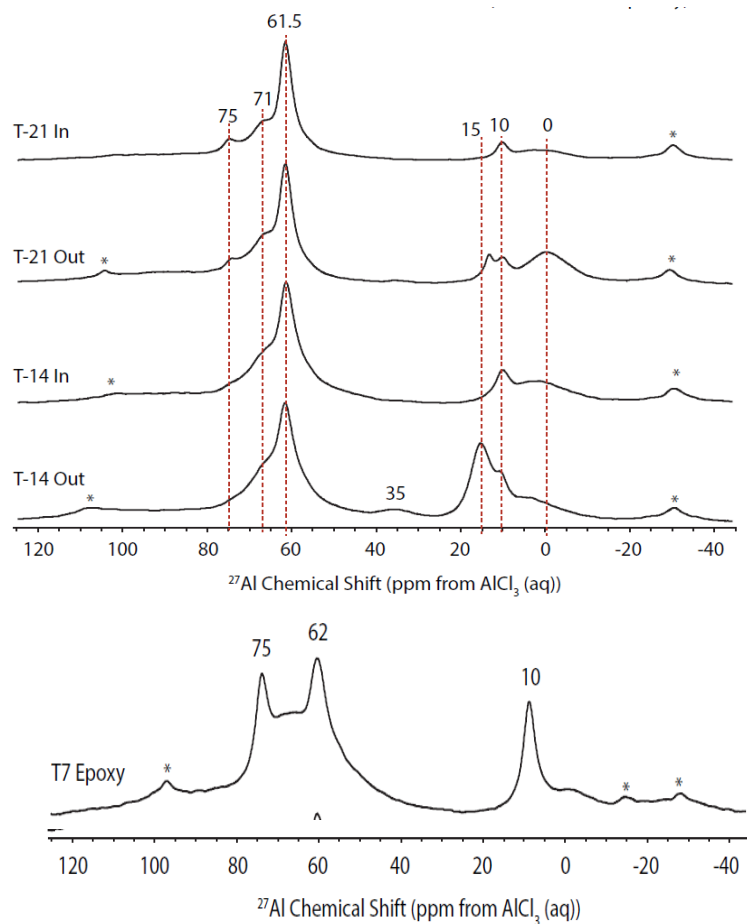
Figure 3-8 -^{27}Al DP NMR spectra of the inner and outer portions of the T21 and T14 monoliths and an example spectrum of an un-leached monolith, T7 from Asmussen et al. (2016).

All samples exhibit a broad asymmetrical line shape in the ^{23}Na NMR spectra (Figure 3-9), indicative of Na in a heterogeneous environment. Although subtle differences exist, the complexity of these samples precludes unambiguous determination of the structural factors giving rise to the differences in [23]Na spectra.

.

CastStone Series
^{23}Na Direct Polarization
17.6T (750 MHz ^{1}H Frequency)
April 2016

^{23}Na Chemical Shift (ppm from NaCl (aq))
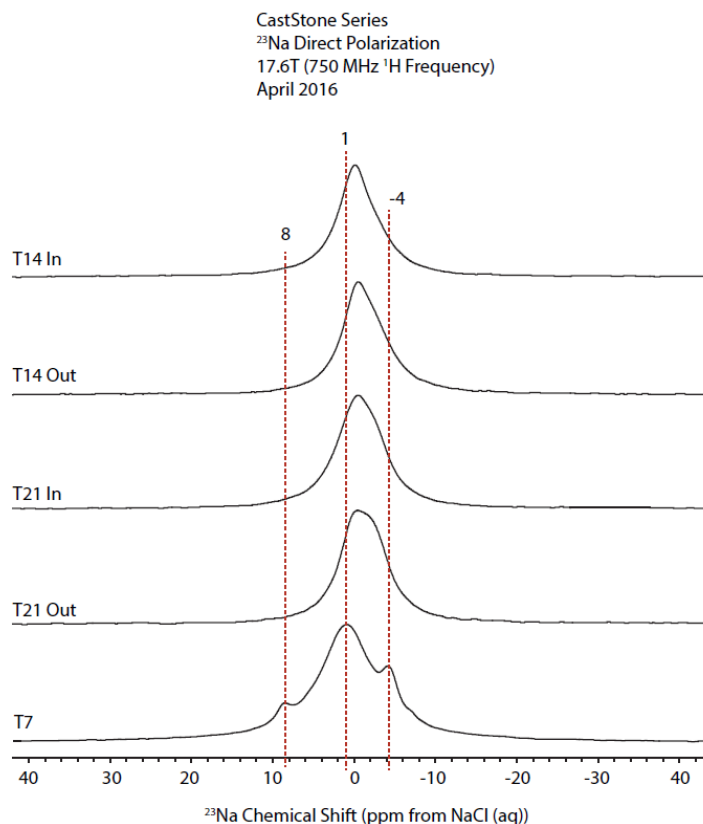
Figure 3-9 – ^{23}Na DP NMR spectra of the inner and outer portions of the T21 and T14 monoliths and an example spectrum of an un-leached monolith, T7 from Asmussen et al. (2016).

These NMR results represent a first-of-a-kind investigation of Cast Stone samples using NMR and hold intrigue, as clear differences in the structural Al bonding develop over time due to contact with the leaching solution. Further characterization of additional long-term leached Cast Stone monoliths using NMR will provide additional insight into this Al bonding transformation process that may impact contaminant leach rates.

3.4.3   Scanning Electron Microscopy (SEM)/X-ray Energy Dispersive Spectroscopy (EDS) Imaging

SEM imaging was performed on selected monolith pieces to determine differences resulting from composition and leaching variances. The micrographs in Figure 3-10 a) and b) display the general surface profile of the T5-DI monolith. An image in Figure 3-10 c) of the surface shows heterogeneity and several sites were selected for elemental analyses with EDS. The spots are color and letter coded. The points of highest interest are A and C at which Tc was detected. This Tc on the outer surface of the monolith and isolated in these regions shows release from the monolith occurs at distinct locales. These sites contained more Ca and less Si and Al than the other sites on the surface. It should also be noted that Sn is detected at these regions containing Tc, and Sn was not previously reported to be a component of the dry blend or LAW simulants used, thus the contribution from Tc at these locations may be higher (i.e., the Sn signal may in fact be "slightly distorted" Tc energy signal)
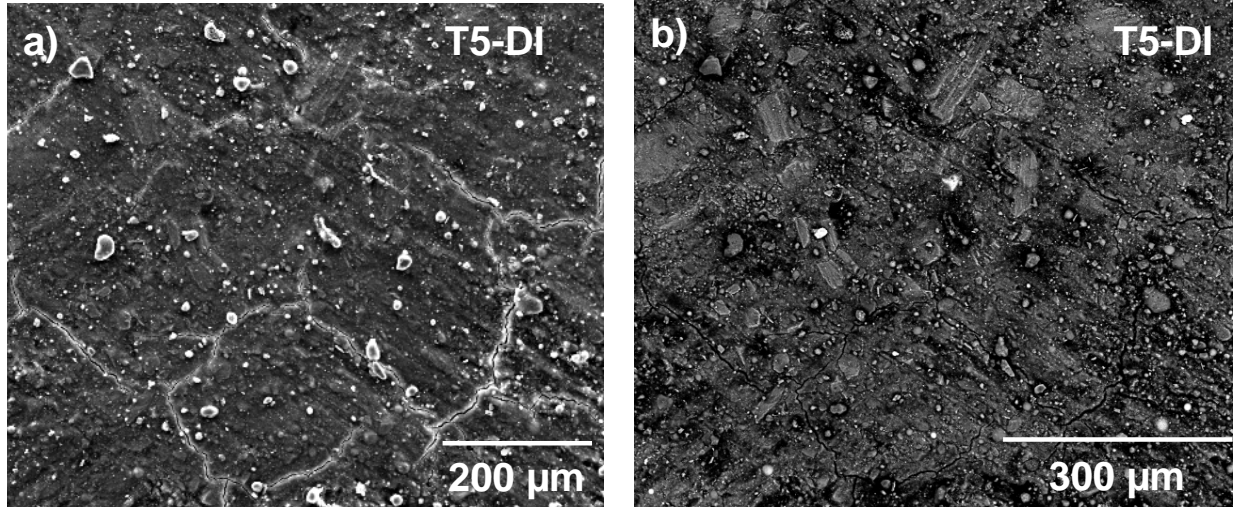
Element (wt%)	A	B	C	D	E	F	G	H
NaK	2.6	1.9	1.9	3.1	4.9	2.7	4.0	4.6
MgK	4.8	15.4	2.2	9.6	6.5	8.2	7.4	26.7
AlK	2.8	10.6	2.2	13.6	8.6	4.5	4.6	16.8
SiK	5.2	29.3	3.8	16.4	18.5	6.4	10.4	24.1
PK	1.7	0.2	1.7	0.9	2.2	0.2	0.2	0.1
SK	1.1	1.1	1.1	0.5	0.7	0.3	0.5	0.4
TcL	2.2	0.0	2.3	0.6	0.8	0.1	0.1	0.0
KK	1.1	0.7	1.0	0.2	0.7	0.3	0.4	0.6
SnL	3.5	0.7	3.7	0.6	0.9	1.4	1.1	0.5
CaK	70.5	36.1	75.7	39.5	50.1	73.7	68.2	18.3
BaL	2.0	0.4	1.6	0.2	1.9	0.7	0.8	0.3
TiK	0.5	0.6	0.6	5.2	0.4	0.0	0.2	0.7
CrK	0.8	0.2	0.9	0.1	0.2	0.1	0.2	0.1
FeK	1.4	2.7	1.2	9.5	3.7	1.6	1.7	6.8

Figure 3-10 – a) SEM micrograph (secondary electron mode) of the T5-DI outer wall, b) SEM micrograph (backscatter mode) of the same area on the T5-DI sample, c) SEM image showing the locations (colored and numbered) selected for EDS measurements and the corresponding values at each location.

Viewing the T5-VZ surface in Figure 3-11 (the aragonite/calcite outer film was manually scraped off prior to imaging), a clear difference in the morphology can be seen compared with T5-DI. The surface roughness is higher in Figure 3-11 a), compared with 3.10 a), and several long crystalline particles are present in the magnified image (Figure 3-11 b). EDS spot analyses of the areas marked in the micrograph (Figure 3-11 c) show a higher number of Ca rich sites on the surface. This increased Ca is likely a result of residual aragonite/calcite outer film on the surface that was not effectively scraped off. Locations C, F and G contain significant levels of Tc, similar to the heterogeneous Tc on the T5-DI surface. Locations D and H are likely Ca-O and Mg-O phases respectively.
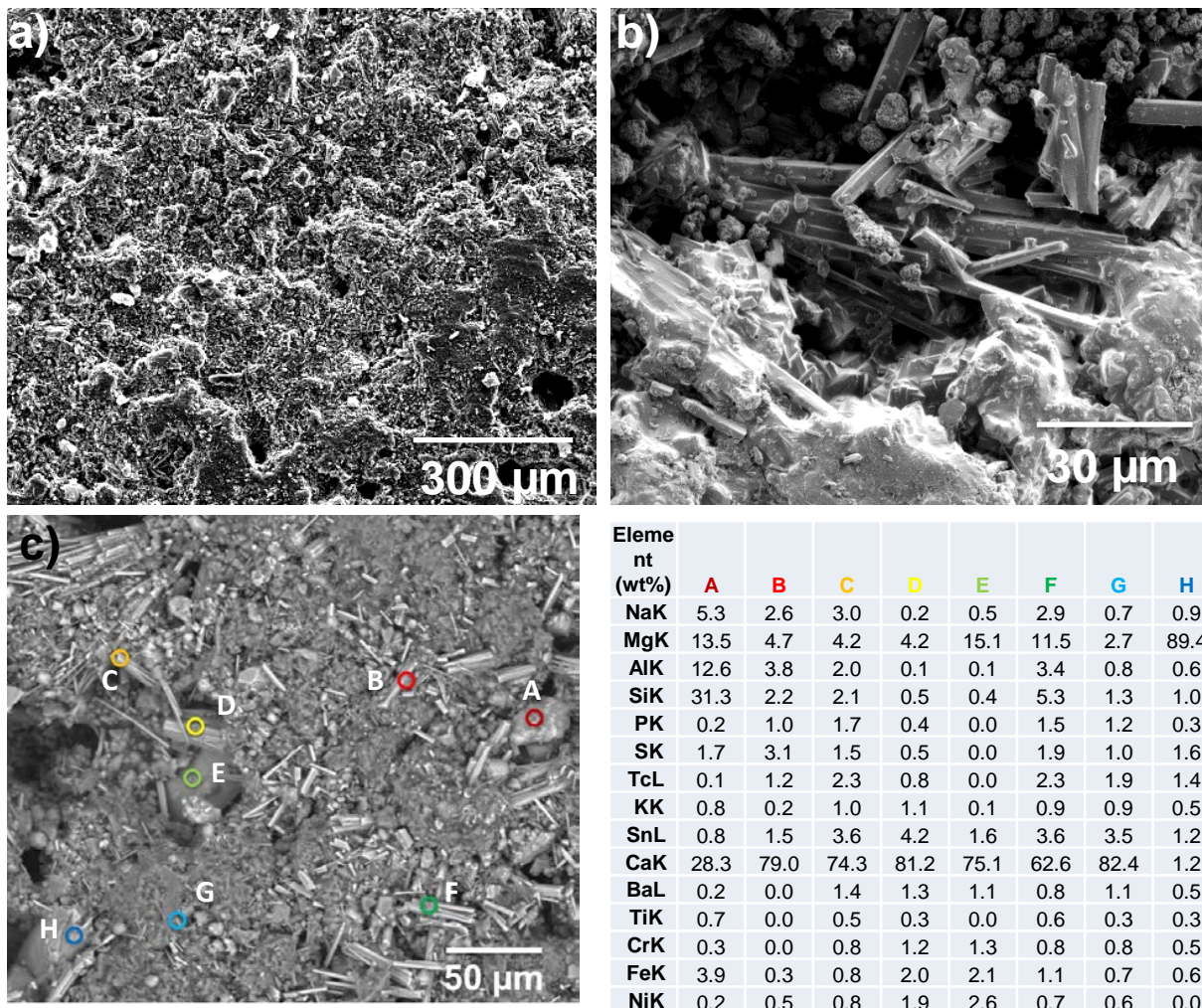
Figure 3-11- a) SEM micrograph of the T5-VZ outer wall, b) magnified view of the T5-VZ surface, c) SEM image showing the locations (colored and numbered) selected for EDS measurements and the corresponding values at each location.

The T17 monolith SEM micrographs can be seen in Figure 3-12. The general surface of T17 appears very similar to the T5-DI monolith, which was also leached in DIW (Figure 3-12 a and b). EDS spot analyses (Figure 3-12 c) showed two Fe-rich regions (spots A and B), a Si-rich particle (spot C, likely residual fly ash), and the general surface containing Ca and Si. No Tc "hot spots" could be found on the T17 monolith surface.

Element (wt%)	A	B	C	D	E
NaK	0.7	1.7	0.7	2.6	3.8
MgK	1.1	1.5	0.7	4.0	1.8
AlK	9.3	4.3	8.6	10.8	9.4
SiK	9.2	6.9	76.5	33.5	42.2
PK	0.2	0.1	0.1	1.1	0.3
SK	0.2	0.1	0.1	0.2	0.3
KK	0.7	0.4	3.4	2.4	1.7
CaK	2.2	4.0	0.7	40.2	38.7
TiK	0.4	0.4	0.3	0.8	0.3
FeK	76.1	80.7	8.8	4.4	1.5
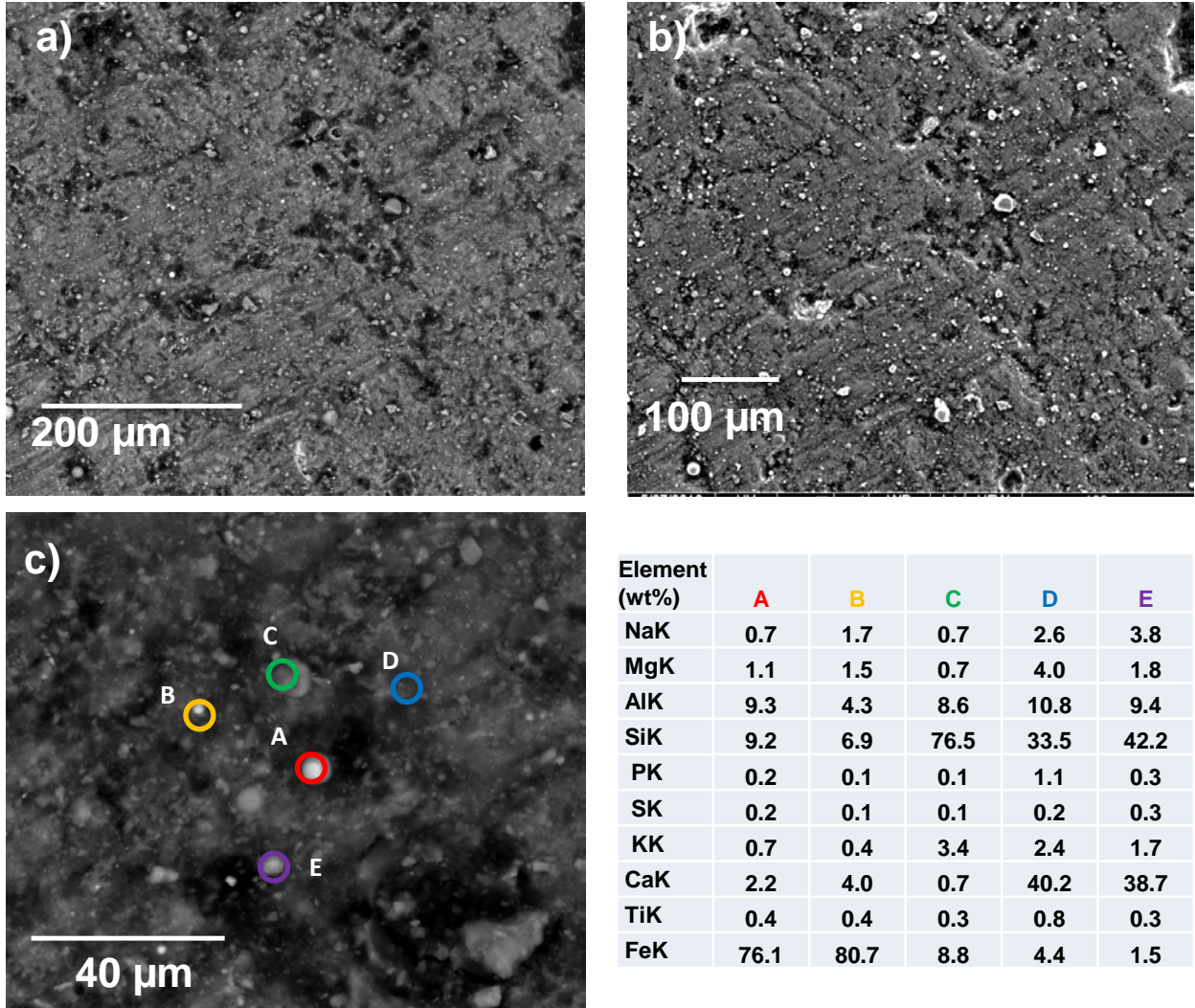
Figure 3-12 - a) SEM micrograph (backscattered electron mode) of the T17 outer wall, b) SEM image (secondary electron mode) of the same area on the T17 outer wall. c) SEM image showing the locations (colored and numbered) selected for EDS measurements and the corresponding values at each location.

3.4.4   Digital Autoradiography

Identifying radionuclide locations in Cast Stone monoliths is difficult due to their presence at concentrations below the detection limit for most solid phase characterization techniques and their heterogeneous distribution. Thus, further identifying mineralogical composition of areas concurrent with the radionuclides is also challenging. Being able to identify the evolution of the radionuclide distribution, and the mineral phases with which they associate is imperative to the long-term performance prediction of the Cast Stone waste form. Single particle digital autoradiography (iQid) presents a novel approach to the age old autoradiography technique that allows for accurate and rapid identification of radionuclide distribution within Cast Stone. Further information on the development and use of the iQid technique can be found in a previous publication (Miller et al. 2015). Cross sectioned "pucks" from the long-term leached monoliths, Figure 2-1, were sealed in a mylar film and analyzed with the iQid system.

Figure 3-13 shows the iQid β-activity maps resulting from performing digital autoradiography on the following monolith pucks: a) T5-DI, b) T5-VZ, c) T10 and d) T17 monoliths. The pucks were taken from section B of the monoliths (the unstained surface from the phenolphthalein testing). The intensity scale bar in the images corresponds to the relative number of β-decay events occurring at the specific pixel. ^{99}Tc is the sole source of β-radiation in the monoliths, thus a higher signal from a region corresponds to a higher concentration of Tc. Both T5-DI and T5-VZ show an enhanced ring of β activity near the outer edge of the monoliths, with a higher signal arising in the T5-DI sample. This concentration of Tc in the outer ring may be a result of the long-term leaching of the monoliths and Tc migrating toward the outer wall.
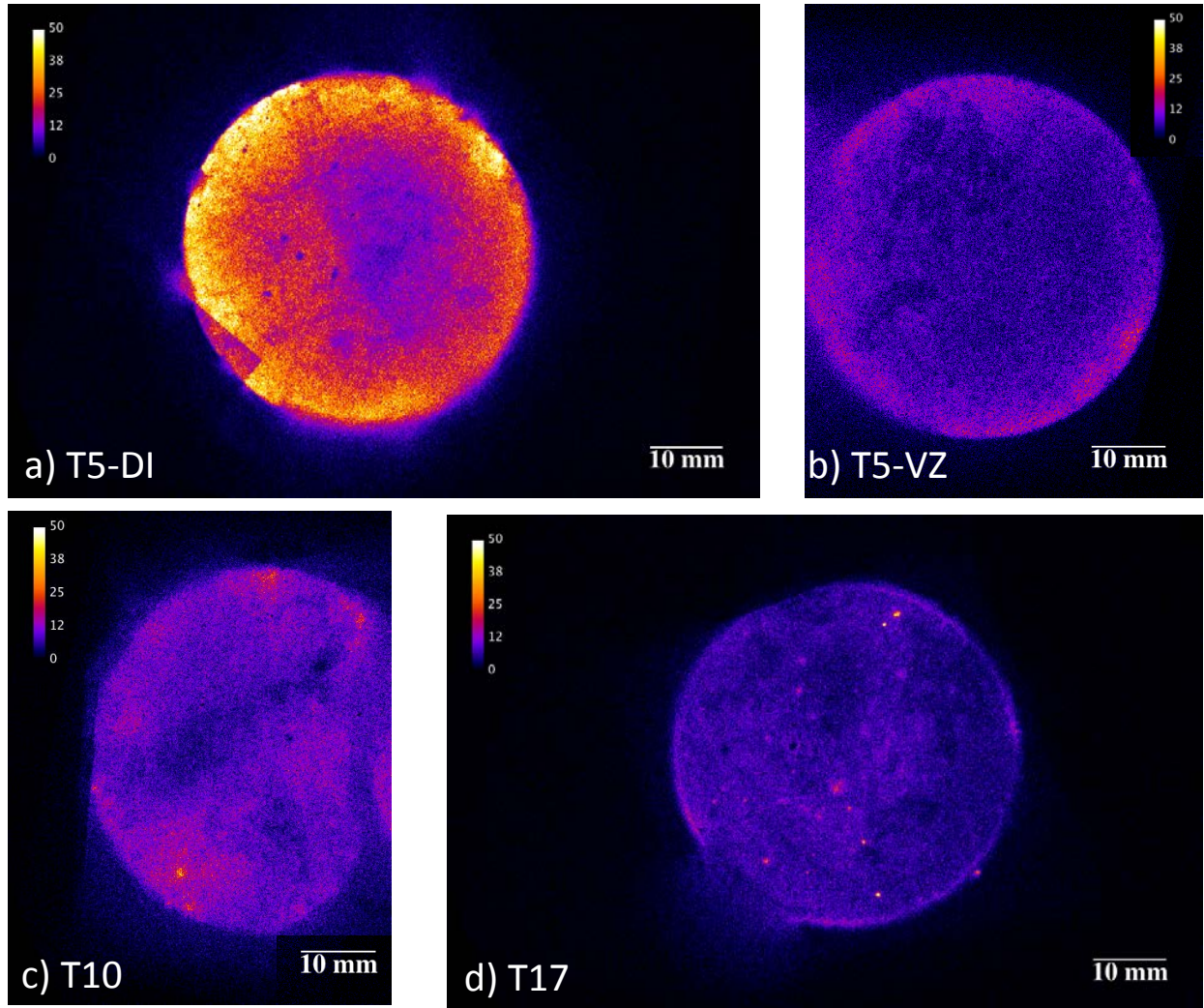
Figure 3-13– Digital autoradiography β decay maps of the monolith cross-sections of a) T5-DI, b) T5-VZ, c) T10 and d) T17. The color contrast is a measure of the relative number of β decays detected at that specific pixel, corresponding to the location of Tc in the monolith. Each sample was monitored for 45 h.

Figure 3-14 shows the Al, Si, Ca and S elemental maps and the β-activity map resulting from a small section of the T5-DI monolith. The Tc is distributed evenly over the small scale of this sub-sample. There is small scale heterogeneity in the elemental maps for Al, Si, Ca and S but it is not possible to discern if Tc is preferentially associated with any of these areas, given the resolution of the iQid system. There is,

however, a pore visible in the sample as shown by the white circle. The pore contains high concentrations of Ca and S and low concentrations of Al and Si supporting the previous data suggesting the presence of ettringite in the pores. The β-activity map shows that no Tc is present in the pore, indicating that these pores do not represent a preferential pathway for Tc out the monolith at this stage in the leaching process.
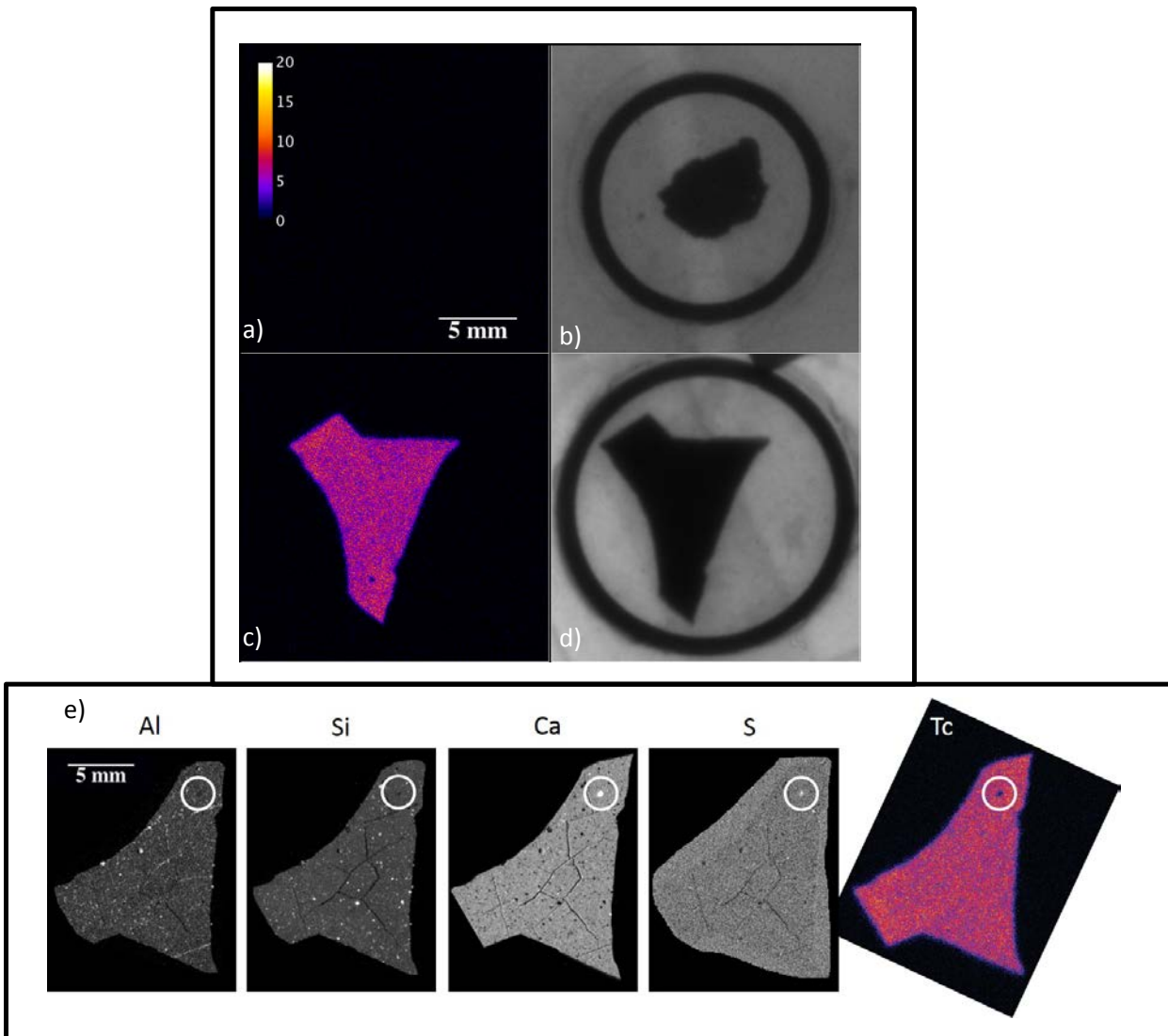
Figure 3-14- a) iQid β decay map of a non-spiked monolith sample, b) shadow image showing the sample prior to iQid imaging, c) iQid β decay map of a sample from the T5-DI monolith, d) shadow image showing the T5-DI sample on the detector prior to the iQid imaging and e) Micro-XRF of a sample from T5-DI (shown in c and d) showing elemental maps for Al, Si, Ca and S Kα intensity and the digital autoradiography β decay map corresponding to Tc.

For the T10 and T17 monoliths, which were fabricated in a different Cast Stone dry blend-waste simulant batch than the T5 monoliths, a far different distribution of Tc was identified. In the T10 monolith, Figure 3-13 c), some increased β signal was observed at portions of the outer edge of the sample, however the Tc appears to be congregating in discrete locations within the monolith. A Tc "hot spot" can be clearly seen in the bottom-left of this monolith's cross-section and two other discrete Tc hot spots occur on the top of the image. A higher number of Tc "hot spots" can be seen in the T17 monolith

in Figure 3-13 d). These Tc "hot spots" on the T17 cross-section are spread through the monolith, with an incomplete ring also appearing at the outer edge. At this point, these measurements are qualitative and give information on the spatial distribution of Tc in the samples. Future work will develop standards to determine Tc concentration at specific locations and analyze these areas with µXRF and SEM/EDS.

The iQid system can also analyze α-radiation from samples. Figure 3-15 shows the T17 monolith analyzed for α-decay resulting from the ^{238}U added with the waste simulant (Westsik et al. 2013). The α-radiation image is not as clear as the β images as the number of α-decays over a set exposure time is less than the number of β-decays, given the longer half-life of ^{238}U. The α radiography image is overlaid on a shadow image of the sample to ensure that the signal was arising from the monolith and not from the background. There are three hot spots arising from the U present in the T17 monolith cross section. This shows that the U is isolated in distinct regions of the Cast Stone and was not evenly distributed suggesting that the uranium present in the liquid waste simulant has precipitated or become associated with discrete solids in the Cast Stone.
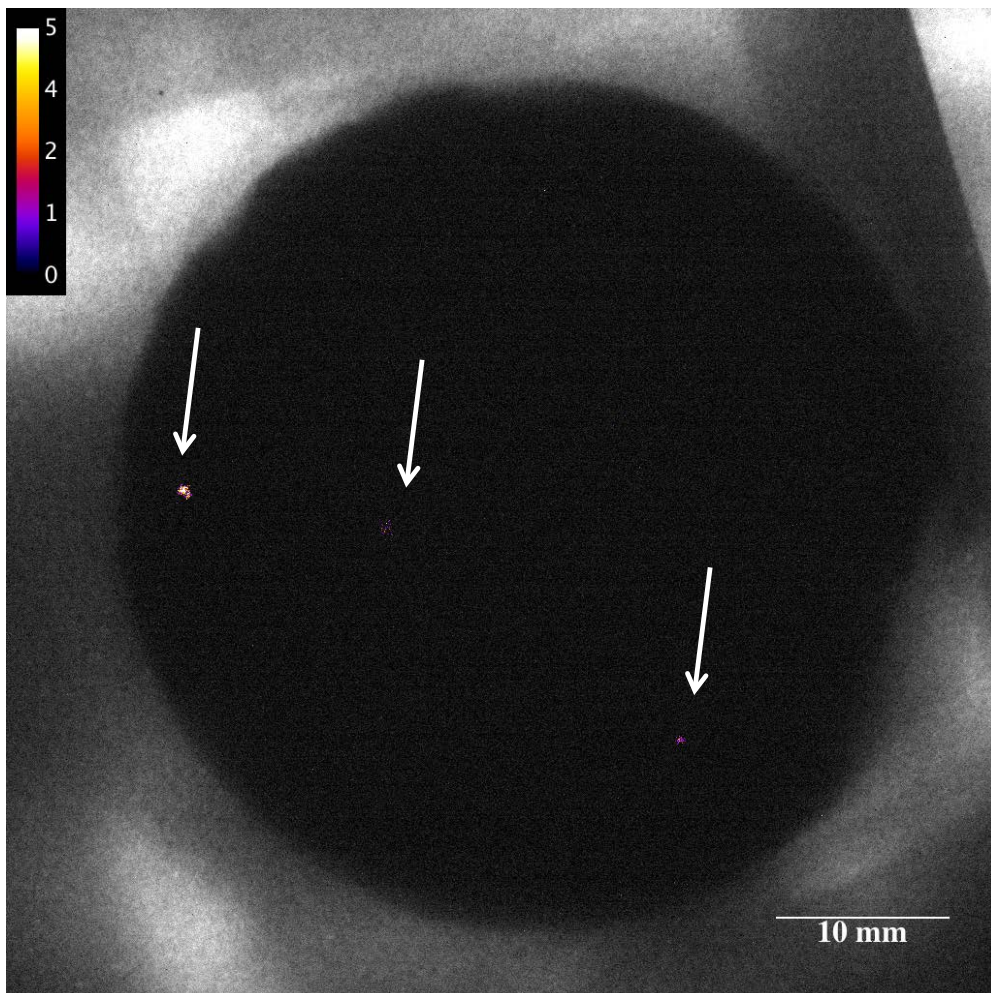
Figure 3-15 - Digital autoradiography α decay maps of the T17 monolith cross-section. The color contrast is a measure of the relative number of α decays detected at that specific pixel, corresponding to the location of U in the monolith. The sample was monitored for 45 h. The radiograph is overlaid on a shadow image taken following the detection to ensure the signal was coming from the monolith sample. The white arrows show the α "hot spots".

3.4.5   Biological Characterization

The T18LCS-7.8RIS-3 monolith exhibited biological growths similar to many long-term leached monoliths in VZPW, the growths can be seen in Figure 3-16 a). Samples of the biological growths from this monolith were removed from the monolith while it was still present in its archived leaching solution. Because the six monoliths subjected to detailed solid phase characterization had already been removed from their final leachates and dried to avoid any alterations resulting from the biological growths being outside of an aqueous environment, the biological characterization was performed on monolith T18LCS-7.8RIS-3 immediately after its removal from solution. Following removal of low quality sequences, approximately 84,000 and 93,000 sequences were analyzed for the T18 sample. For comparison, we present a similar characterization of a biological growth from a 63-day leached Cast Stone sample in VZPW (T6-5) from Asmussen et al (2016). Phylogenetic analysis of the samples showed very low diversity with four or fewer phyla being represented in the samples, Figure 3-16 b). *Proteobacteria* were the most dominant phylotype, especially for the T6-5 sample. Interestingly, the number of *Proteobacteria* decreased over time when comparing T6-5 (63 d leach) to T18LCS2-3 (971 d solution contact), while the number of *Firmicutes* and *Actinobacteria* increased in the T18 biological material. Sequences representing the phylum *Armantmonadetes* became dominant in the T18LCS2-3 sample, while very few sequences of this phylum were found in sample T6-5.
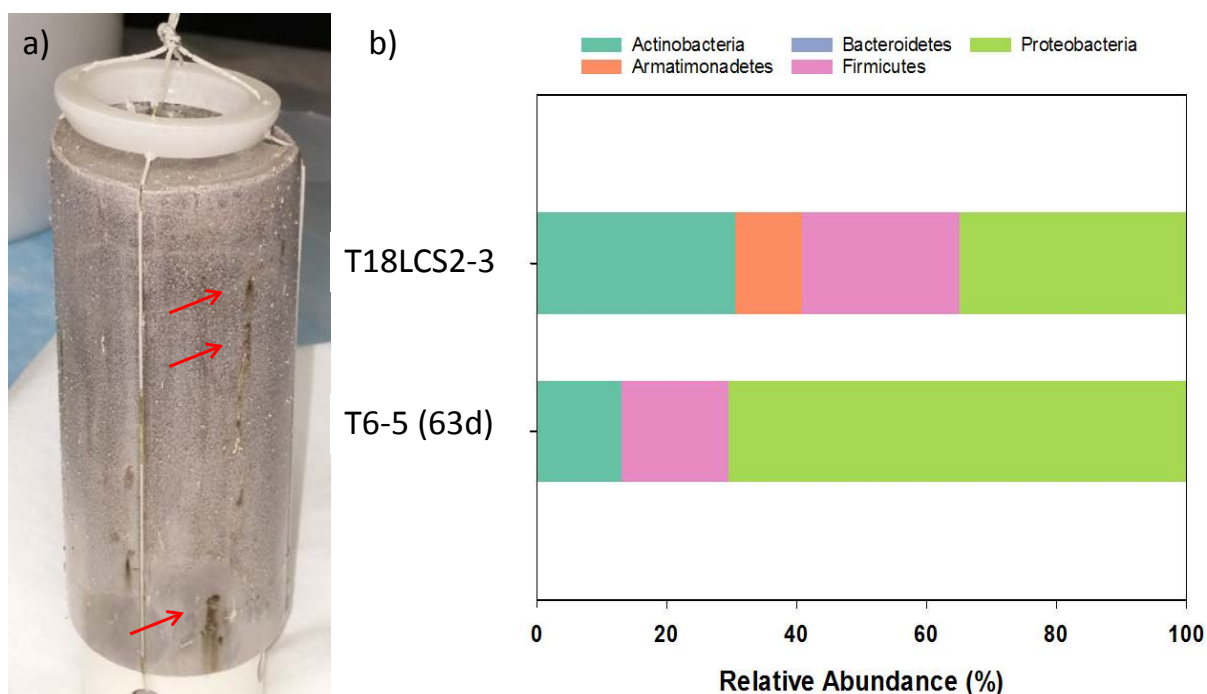
Figure 3-16- a) photograph of the T18LCS2-7.8RIS-3 monolith immediately after removal from its archived VZPW leaching solution, several biological growths are identified with the red arrows and b) relative abundance of bacterial phyla present in precipitates from the T18 sample and compared with T6-5 sample (Asmussen et al. 2016).

Genus level identification within these phyla indicate that the samples are quite different related to bacteria present, in fact, only *Brevundimonas* is present in both samples, and actually increased when comparing T6-5 to T18LCS2-3 (Table 3-2). Bacterial genera representing greater than 10% of the community are described in the table. Bacteria related to those found in the Cast Stone growths (black spots on monolith surfaces) have shown the ability to grow oxidatively on a range of carbon sources, and

may be able to metabolize the acetate present in Cast Stone LAW simulant. Likewise, a number of the bacteria found, are halotolerant and some combine this phenotype with tolerance to alkaline conditions. Both of these characteristics would allow the bacteria to grow in the high salt, alkaline environment on the surface of the Cast Stone. Finally, resistance to metals, and the ability to use inorganic constituents in the waste including nitrate and radionuclides, in addition to oxygen would allow these microbes to grow on the surface of the Cast Stone.

Table 3-2 Bacterial genera found in Cast Stone precipitates and description of phenotypic characteristics

Genus	Abundance (%) T-6-5	T-18LCS2-3	Description
Brachybacterium	0	30.4	*Actinobacteria*. Aerobic, halotolerant, chemoheteroroph isolated from oil brines and other high salt environments
Solirubrobacter	12.6	0	*Actinobacteria*. Aerobic, chemoheterotroph isolated from soils and sediments. Dessication and possible radioresistance
Armatimonadetes (Phylum)	<1	10.3	Aerobic, chemoheterotroph isolated from diverse environments
Bacillales (Order)	2.4	0	
Bacillus	6.0	<1	
Geobacillus	1.4	0	
Salinococcus	6.5	0	
Staphylococcus	<1	24.2	*Firmicutes*. Facultative anaerobes, chemoheterotrophic. Primarily known for pathogenicity, but there are non-pathogenic species that show ability to grown on a range of organic substrates
Brevundimonas	16.2	34.8	*Proteobacteria*. Facultative anaerobe, chemoheterotrophic (oligotrophic), halotolerant, alkaliphilic. Isolated from diverse environments. Some species have shown resistance to ionizing radiation.
Cupriavidus	30.7	0	*Proteobacteria*. Facultative anaerobe, chemoheterotroph/chemolithotrophic. Commonly found in soils. Known for resistance to metals, some strains have demonstrated the ability to chemically reduce metals.
Ralstonia	23.5	0	*Proteobacteria*. Facultative anaerobe, chemoheterotrophic. Isolated from numerous environments including soil and water. Resistant to metals, able to chemically reduce a variety of metals and metalloids.

4.0   Summary

This report, together with the report by Asmussen et al. (2016), includes the first investigations into characterizing Cast Stone monoliths that were leached for a relatively long time; the monolith leaching began in early July 2013 and continued through late February 2015. A recent revision to the report covering the extended leach testing of the monoliths from this suite has been published, (Serne et al. 2016) and it was noted that long term diffusivity measurements (> 63 day) may not accurately predict release rates of contaminants as a depletion of the waste form initial inventory and physical changes have occurred (e. g. aragonite formation on the monolith's outer surface for those leached in VZPW, and rubblization of a few monoliths). Identifying techniques for successfully characterizing solid state changes in these Cast Stone samples would help in identifying contaminant release mechanisms needed to support the long-term waste form performance assessments (PA). Information obtained from a variety of techniques used and reported herein includes: (i) penetration of separate carbonation and oxidation fronts; (ii) identification of secondary minerals formed during leaching/weathering; (iii) changes in the chemical environment of key elements in the waste form; (iv) identifying radionuclide distributions within discrete localized regions of the monolith; and (v) elucidating possible mechanisms that control radionuclide and contaminant release.

Six Cast Stone monoliths fabricated with LAW simulants were selected from the monoliths that were stored in their final leaching solution after ~2 years of continual leaching using the EPA Method 1315 protocol. After removal from their final leachate for about an additional year, the leached monoliths were either immediately sectioned in the open atmosphere for spectroscopic characterization (T14 and T21) or immediately moved to an anoxic chamber for sectioning into pieces of known location relative to the monolith's final dimensions for oxygen/carbonation front measurements, followed by spectroscopic investigations (T5-DI, T5-VZ, T10 and T17). The purpose of placing and sectioning the four monoliths in the anoxic chamber was to avoid artificially influencing the O_2 and carbonate ingress results due to atmospheric exposure. During the EPA Method 1315 leaching, these monoliths were exposed to fully water saturated conditions in the open atmosphere, and these results are most relevant to such conditions. Future work should be focused on performing similar experiments on monoliths exposed to partially water saturated conditions, relevant to eventual IDF conditions.

The monoliths placed into the anoxic chamber (T5-DI, T5-VZ, T10 and T17), were first sectioned horizontally into disks and did not show a distinct color change front after treatment with phenolphthalein. Small isolated regions within the monoliths did not undergo a color change after phenolphthalein staining (indicating significant carbonation had occurred in very localized regions). Yet each monolith cross-section showed complete phenolphthalein staining to their outer edge suggesting incomplete carbonation. This result indicates that the overall pH of the monoliths was not significantly reduced by carbonation reactions during extended leaching periods in either DIW or VZPW.

The T21 monolith, which was not sectioned into disks for the phenolphthalein staining, suggests different localized carbonate ingress processes can occur within the Cast Stone monoliths. T21 was leached in VZPW and an outer film of aragonite/calcite was formed over time. Manually sectioning the T21 monolith revealed an outer shell, (~5 mm thick) that easily broke away from the monolith at a similar depth. A white deposit was observed at the interface between the outside of these naturally rubblized pieces and the inner core of the remaining monolith, which XRD identified as a mixture of ettringite (~60 %) and calcium carbonate (~20%). Also at this depth, pores were observed to be filled with this deposit but such white deposits were not seen in the interior of the monolith. A hypothesis drawn from these findings would suggest that carbonate does enter the monoliths over time (from the VZPW where it is a component, or from dissolved CO_2 in DIW) and moves very selectively through portions of the porous network. At the same time, the monoliths are beginning to dissolve releasing Al, Si, Ca, SO_4^{2-} etc. into the

internal Cast Stone pore liquid. These two processes are not capable of overcoming the overall alkalinity of the bulk grout during the leach times (a few years) that these monoliths endured. However, within select pores the presence of these species, in combination with carbonate at high pH, led to the deposition of carbonates and the formation of ettringite. Formation of secondary minerals such as ettringite and calcium carbonate after hardening of the Cast Stone results in a volume increase and can create internal pressure on the monoliths bulk structure, producing micro-cracks within its structure. This volume increase/micro-cracking was observed in the T21 monolith as the "outer skin" broke away easily from the surface, and upon removal from solution large pieces of the T21 monolith had cracked off exposing the ettringite/carbonate white deposit at the break point. As the phenolphthalein staining was performed on a small set of monoliths, and the carbonate ingress/deposit growth was only observed in one monolith, this cannot be concluded to be a general trend until a comprehensive study of additional monoliths from similar batches is undertaken.

In our short-term DIW leach testing of sectioned aliquots of the Cast Stone to evaluate O_2 front penetration, a small increase in %Tc and %Cr released was observed moving from the outer wall of each monolith to the interior of each monolith. This is contradictory to the observations in the single face studies in partially water saturated and atmospherically exposed Cast Stone monolith studied at SRNL. During the 3 + years of water saturated exposure our leached monoliths appear to show little oxygen ingress into the monolith. The reductive environment within the Cast Stone interior is still present, best shown by the limited Cr release in the short-term DIW leach test.

The I K-edge XAS analysis of the T21 monolith (highest levels of starting I as iodide in our long-term leached monoliths) also supports the retention of reducing conditions within the Cast Stone, confirming that I in the monolith exists as iodide with no detectable conversion to iodate, the oxidized form of iodine. Under oxidizing conditions, it is plausible that the iodide could be oxidized to iodate.

The T21 and T14 monoliths were analyzed with solid state NMR spectroscopy in both the [27]Al and [23]Na modes. Na being a large component of the Cast Stone and Al a key element in the bonding of the cementitious waste form make them viable candidates for analysis. The [23]Na mode did not display any clear differences between the monoliths inner and outer portions. The [27]Al mode showed differences in the local environment of the Al between the inner core of the monolith and Al in the outer wall. The inner core and outer wall samples, from both monoliths that were characterized in detail contained similar tetrahedrally coordinated Al. However the samples from the long-term leached monoliths' outer wall contained Al in octahedral coordination that was not present in unleached Cast Stone. Without further analyses of more Cast Stone samples (both unleached and leached), the impact of this difference in Al bonding on leaching behavior of COPCs cannot be determined, although it is clear that the structure of the Cast Stone is being altered throughout the leaching period relative to distance from the solution contacting face.

XRD analyses showed compositional differences between the mineralogical makeup of the various monoliths, and also between the inner and outer portions of each monolith. All the monoliths had a large amorphous component, and the crystalline portion was characterized quantitatively using rutile as an internal standard. The interior of all the monoliths, except T17, showed a higher portion of tobermorite, a calcium silicate hydrate common in hydrated cement. Calcite and brucite were found in higher concentrations on the outer wall samples, especially those monoliths leached in VZPW, which contained relativel high concentrations of dissolved bicarbonate. Sodalite was found in T14 and T21 and in the inner portion of T5-DI, with evidence that this was transforming to cancrinite on the outer wall as shown in T21, T14, T5-DI and T17. These results re-affirm the heterogeneity between samples and between the different regions (interior vs. outer wall) of the Cast Stone. Upon complete curing, the Cast Stone should have an even chemical and mineralogical distribution, yet the minerals are transforming into more thermodynamically stable phases throughout the leaching process.

Variations in the morphology of the monoliths leached in VZPW and DIW were also observed using SEM/EDS analyses. This is not unexpected with the formation of the outer deposit on the VZPW leached monoliths and the difference in leachate pH between the DIW and VZPW (i.e. ~12 vs. ~10). Discrete locations on several monolith surfaces were characterized with EDS and found to contain Tc, while others were absent of Tc. This would be indicative of Tc leaching through specific sites within the monolith out into the leach solution.

The most telling measurement of the variation of the distribution of contaminants within the Cast Stone monoliths is from the radiography of the samples. Analyzing entire monolith cross-sectioned surfaces (faces of a cut puck) showed the distribution of Tc and U (for T17) in the monoliths with real time detection of β and α decays, respectively. The T5-DI and T5-VZ monoliths, fabricated as part of the Tc-gluconate Suite of monoliths (Serne et al. 2015, 2016), displayed the strongest β signal from the outer ring of these monoliths. The β signal corresponds to the location of Tc within the monolith. Throughout the extended leaching time, the Tc appears to be migrating and congregating in this outer region near the monolith wall. On a small scale, Tc distribution was relatively homogenous although it was not present in the ettringite- and calcium carbonate-containing pores. Some Tc localizing in the outer ring of the monolith was also observed in the T10 and T17 monoliths although Tc localization in the T10 and T17 cross sections was more of a sporadic distribution on their outer walls. For the T10 and T17 monoliths the majority of the Tc appeared to have localized in discrete regions, ~ 50-100 µm in size, within the monoliths' interior.

In the T17 monolith, the U inventory was observed to also congregate in discrete very localized regions, through monitoring of the α-decay. The compositional differences (e.g., LAW simulant composition, source of dry blend materials, and water-to-dry blend) of the T5 set and T10/T17 Cast Stone monoliths are not large, and yet these monoliths show significantly different Tc distribution. In modelling contaminant release from cementitious waste forms, using observed effective diffusivities, a homogenous distribution of the contaminant within the monolith is assumed. These radiography images, for the first time, suggest this homogeneity assumption is not the case and that the radionuclides are present in discrete locations or are beginning to congregate in a ring near the outer wall of most monoliths. No conclusive statement on the origin of these isolations, nor their time of formation, can be made from these initial autoradiography measurements. Identification of the mineral and elemental make up at these discrete "hot spot" locations was not in the scope of this work. Such work is warranted, and should be carried out on the additional archived long-term leached monoliths, to begin to decipher, to understand, and to predict this radionuclide behavior in the Cast Stone monoliths.

Biological growths on the long-term leached monoliths were identified to be a mixture of *Proteobacteria, Actinobacteria, Armatimonadetes* and *Firmicutes*. Compared with the growths on a 63 d leached monolith (Asmussen et al. 2016), the amount of *Proteobacteria* has markedly decreased on the long-term leached monolith and there is a concurrent increase in *Actinobacteria* and *Armatimonadetes*. It is unclear at this time what effect the biological growths have on the performance of the Cast Stone.

The initial characterizations presented in this report show regions of the Cast Stone monoliths to be altering based on the position relative to the monoliths interface with the leach solution. Much work was done to confirm that a combination of SEM/EDS, NMR, XRD and iQid to study the Cast Stone samples can provide valuable insight needed to predict their long-term behavior. It was clearly observed that the monolith structure, composition and radionuclide distribution were being altered as the waste form weathered/aged in the water saturated EPA Method 1315 leach tests. No quantitative statements on the rates of these processes can be made at the current time due to the small number of monoliths investigated. However, the initial groundwork has been laid to develop a systematic study of more of the remaining archived monoliths to understand the unique features observed in this report. As a result, the

authors propose the following questions or protocols that can be addressed or used, respectively in future work:

i) How does the radionuclide distribution within the monoliths change with time?

ii) Compositional identification of Tc isolations in the Cast Stone using the radiography map to focus SEM/EDS/XRF analyses on these regions.

iii) For the monoliths studied in this work, all have one (and in some cases two) monoliths from the same batch archived in their final leachates that can now be characterized effectively with equipment and procedures described herein. Analyzing these additional long-term leached monoliths will allow for insight as to whether the trends observed are compositional effects, batch specific, monolith specific or due to the composition of the solutions used for the leaching. Also analyzing "un-leached" monoliths from similar monolith sets would provide a suitable control.

iv) A combination of radiography, SEM/EDS and XRF of "hot spots", NMR, XRD and XAS should be applied in future solid phase characterizations, with additional leach tests continued using the imaged monoliths.

v) Short-term DIW leach to evaluate re-oxidation rates should be performed on identical pieces of Cast Stone under both anoxic and aerobic environments to determine the effect of exposure to air significantly impacts release of redox sensitive species.

References

Almond, P, D Kaplan, C Langton, D Stefanko, W Spencer, A Hatfield and Y Arai. 2012. "Method Evaluation and Field Sample Measurements for the Rate of Movement of the Oxidation Front in Saltstone." *SRNL-STI-2012-00468*.

Asmussen, RM, CI Pearce, AJ Lawter, JJ Neeway, BW Miller, BD Lee, N Washton, JR Stephenson, RE Clayton, ME Bowden, EC Buck, E Cordova, BD Williams and N Qafoku. 2016. "Getter Incorporation into Cast Stone and Solid State Characterizations." *PNNL-25577* Pacific Northwest National Laboratory(Richland, WA, USA).

ASTM. 2009. "Standard Practice for Nitric Acid Digestions of Solid Waste." *ASTM D5198-09* ASTM International, West Conshohocken, PA.

Cantrell, KJ and BD Williams. 2013. "Solubility control of technetium release from Saltstone by TcO2·xH2O." *Journal of Nuclear Materials* 437(1–3): 424-431.

Caporaso, JG, J Kuczynski, J Stombaugh, K Bittinger, FD Bushman, EK Costello, N Fierer, AG Pena, JK Goodrich and JI Gordon. 2010. "QIIME allows analysis of high-throughput community sequencing data." *Nature methods* 7(5): 335-336.

Deng, Y, M Flury, JB Harsh, AR Felmy and O Qafoku. 2006. "Cancrinite and sodalite formation in the presence of cesium, potassium, magnesium, calcium and strontium in Hanford tank waste simulants." *Applied Geochemistry* 21(12): 2049-2063.

EPA. 2013. "Mass transfer rates of constituents in monolithic or compacted granulated materials using a semi-dynamic tank leaching procedure." *Method 1315* US Environmental Protection Agency, Washington, DC(Rev.0).

Kodama, S, Y Takahashi, K Okumura and T Uruga. 2006. "Speciation of iodine in solid environmental samples by iodine K-edge XANES: Application to soils and ferromanganese oxides." *Science of the total environment* 363(1): 275-284.

Kuczynski, J, J Stombaugh, WA Walters, A González, JG Caporaso and R Knight. 2012. "Using QIIME to analyze 16S rRNA gene sequences from microbial communities." *Current protocols in microbiology*: 1E. 5.1-1E. 5.20.

Langton, C and P Almond. 2013a. "Cast Stone Oxidation Front Evaluation: Preliminary Results For Samples Exposed To Moist Air." *SRNL-STI-2013-00541*.

Langton, C, D Stefanko and H Burns. 2013b. Saltstone Oxidation Study: Leaching Method–13092. WM2013 Conference.

McKeown, DA, IS Muller and IL Pegg. 2015. "Iodine valence and local environments in borosilicate waste glasses using X-ray absorption spectroscopy." *Journal of Nuclear Materials* 456: 182-191.

Miller, BW, SH Frost, SL Frayo, AL Kenoyer, E Santos, JC Jones, DJ Green, DK Hamlin, DS Wilbur and DR Fisher. 2015. "Quantitative single-particle digital autoradiography with α-particle emitters for targeted radionuclide therapy using the iQID camera." *Medical physics* 42(7): 4094-4105.

Ravel, B and M Newville. 2005. "ATHENA and ARTEMIS: interactive graphical data analysis using IFEFFIT." *Physica Scripta* 2005(T115): 1007.

Raymond, RE, RW Powell, DW Hamilton, WA Kitchen, BM Mauss and TM Brouns. 2004. <u>Initial Selection of Supplemental Treatment Technologies for Hanford's Low-Activity Tank Waste</u>. Proceedings of WM'04 Symposia. WM-4524/RPP-19763-FP, CH2M HILL Hanford Group, Inc. Richland, Washington.

Serne, J, DC Lanigan, J Westsik Jr, BD Williams, HB Jung and G Wang. 2016. "Extended leach testing of simulated LAW cast stone monoliths." *PNNL-24297, RPT-SLAW-001* Pacific Northwest National Laboratory, Richland, WA, USA(Rev.1).

Stutzman, PE. 2001. "Scanning electron microscopy in concrete petrography." *National Institute of Standards and Technology* 2.

Um, W, HB Jung, G Wang, JH Westsik Jr. and RA Peterson. 2013. "Characterization of Technetium Speciation in Cast Stone." *PNNL-22967* Pacific Northwest National Laboratory, Richland, Washington.

Webb, SM. 2005. "SIXpack: a graphical user interface for XAS analysis using IFEFFIT." *Physica Scripta* 2005(T115): 1011.

Westsik, JH, GF Piepel, MJ Lindberg, PG Heasler, TM Mercier, RL Russel, AD Cozzi, WE Daniel, RE Eibling, EK Hansen, MR Reigal and DJ Swanberg. 2013. "Supplemental Immobilization of Hanford Low-Activity Waste: Cast Stone Screening Tests." *PNNL-22747, SRNL-STI-2013-00465* Rev. 0, Pacific Northwest National Laboratory, Richland, Washington and Savannah River National Laboratory, Aiken, South Carolina.

Zha, X, H Wang, P Xie, C Wang, P Dangla and J Ye. 2016. "Leaching resistance of hazardous waste cement solidification after accelerated carbonation." *Cement and Concrete Composites* 72: 125-132.

Appendix A

Short Term Leach Testing Data Analysis

Appendix A
Short Term Leach Testing Data (Tc)

SAMPLENAME	RESULT	UNITS	Tare Mass of Vial (g)	Mass Sample Added (g)	Mass of DIW Water Added (g)	Sample Mass (g)	Volume Water (mL)	Mass of Tc released (ug)	Mass of Tc released ug / g of sample wet	Median Distance of Piece (mm)	Average Tc Released (ug)	St.Dev	Tc in solid (ug/g dry)	Mass Tc in sample (ug)	Total Tc	% Leached	Avg % Leached	St.Dev
CS-T5-DI-4 Section 1-A	30	ug/L	8.56	9.59	33.61	1.03	24.02	0.7206	0.6996	4.79	0.6967	0.002913	8.34	6.10	6.82	10.57	10.53	0.03
CS-T5-DI-4 Section 1-B	30	ug/L	8.66	9.69	33.51	1.03	23.82	0.7146	0.6938	4.79			8.33	6.09	6.81	10.50		
CS-T5-DI-4 Section 2-A	47.6	ug/L	8.54	9.56	33.55	1.02	23.99	1.141924	1.1195	14.19	1.2442	0.124655	6.7	4.85	5.99	19.05	21.58	2.53
CS-T5-DI-4 Section 2-B	54.1	ug/L	8.58	9.54	33.83	0.96	24.29	1.314089	1.3688	14.19			6.07	4.14	5.45	24.11		
CS-T5-DI-4 Section 3-A	55.1	ug/L	8.56	9.51	33.71	0.95	24.2	1.33342	1.4036	23.68	1.6171	0.213475	6.61	4.46	5.79	23.02	28.13	5.10
CS-T5-DI-4 Section 3-B	84.1	ug/L	8.6	9.67	32.96	1.07	23.29	1.958689	1.8306	23.86			5.18	3.94	5.89	33.23		
CS-T5-VZ-2 Section 1-A	19.4	ug/L	8.63	9.01	33.66	0.38	24.65	0.47821	1.2584	6.8885	1.2340	0.024474	5.74	1.55	2.03	23.59	22.56	1.03
CS-T5-VZ-2 Section 1-B	21.5	ug/L	8.71	9.14	33.33	0.43	24.19	0.520085	1.2095	6.885			6.21	1.90	2.42	21.53		
CS-T5-VZ-2 Section 2-A	76.5	ug/L	8.59	9.59	33.65	1	24.06	1.84059	1.8406	16.34	1.6041	0.236496	5.79	4.11	5.95	30.93	27.58	3.34
CS-T5-VZ-2 Section 2-B	57.3	ug/L	8.73	9.71	33.1	0.98	23.39	1.340247	1.3676	16.34			6.02	4.19	5.53	24.24		
CS-T5-VZ-2 Section 3-A	75.5	ug/L	8.51	9.54	33.81	1.03	24.27	1.832385	1.7790	22.99	1.6979	0.081162	5.04	3.69	5.52	33.21	33.13	0.07
CS-T5-VZ-2 Section 3-B	67.5	ug/L	8.6	9.62	34.05	1.02	24.43	1.649025	1.6167	22.99			4.61	3.34	4.99	33.06		
T10HCS1-3 VZP Section 1-A	21.9	ug/L	8.57	9.64	33.36	1.07	23.72	0.519468	0.4855	2.235	0.4828	0.002689	4.34	3.30	3.82	13.61	13.71	0.10
T10HCS1-3 VZP Section 1-B	20.4	ug/L	8.59	9.6	33.37	1.01	23.77	0.484908	0.4801	2.235			4.22	3.03	3.51	13.81		
T10HCS1-3 VZP Section 2-A	21.2	ug/L	8.7	9.5	33.65	0.8	24.15	0.51198	0.6400	10.925	0.6658	0.025875	5.29	3.00	3.52	14.56	15.37	0.81
T10HCS1-3 VZP Section 2-B	13.8	ug/L	8.6	9.08	33.14	0.48	24.06	0.332028	0.6917	10.925			5.05	1.72	2.05	16.17		
T10HCS1-3 VZP Section 3-A	50	ug/L	8.53	9.52	33.94	0.99	24.42	1.221	1.2333	23.655	1.2789	0.04557	7.78	5.47	6.69	18.25	18.62	0.37
T10HCS1-3 VZP Section 3-B	54.4	ug/L	8.73	9.71	33.57	0.98	23.86	1.297984	1.3245	23.655			7.96	5.54	6.84	18.99		
T17LCS2-6 DIW Section 1-A	33.9	ug/L	8.86	9.82	33.99	0.96	24.17	0.819363	0.8535	3.49	0.8085	0.045009	4.98	3.39	4.21	19.45	19.33	0.11
T17LCS2-6 DIW Section 1-B	32.4	ug/L	8.61	9.62	33.42	1.01	23.8	0.77112	0.7635	3.49			4.52	3.24	4.01	19.22		
T17LCS2-6 DIW Section 2-A	42.4	ug/L	8.67	9.79	33.82	1.12	24.03	1.018872	0.9097	12.275	0.8669	0.04284	4.9	3.90	4.92	20.73	19.80	0.93
T17LCS2-6 DIW Section 2-B	31.5	ug/L	8.63	9.57	34.16	0.94	24.59	0.774585	0.8240	12.275			4.99	3.33	4.10	18.87		
T17LCS2-6 DIW Section 3-A	44.1	ug/L	8.64	9.64	33.91	1	24.27	1.070307	1.0703	22.455	1.0964	0.026046	4.82	3.42	4.49	23.82	24.20	0.38
T17LCS2-6 DIW Section 3-B	48.8	ug/L	8.62	9.67	33.82	1.05	24.15	1.17852	1.1224	22.455			4.85	3.62	4.79	24.58		
Blank-1	ND	ug/L																
Blank-2	ND	ug/L																

Solution concentrations and sam
Vial tare mass, sample mass and
Sample mass (wet) added to vial
Volume of water added to vial co
Total mass of species released i
Mass of species released per gra
Median Distance of piece taken f
Average release of species from
Content of species measured by
Mass of the species present in th

col U = col T*0.71* col M
Total amount of the species; col
% of species leached calculation

col W = col O/col V

Avg % leached of species from t

A.1

Short Term Leach Testing Data (Cr)

SAMPLENAME	ANALYTE	RESULT	RL	UNITS	Tare Mass of Vial (g)	Mass Sample Added (g)	Mass of DIW Water Added (g)	Sample Mass (g)	Volume Water (mL)	Mass of Cr released (ug)	Mass of Cr released ug / g of sample wet	Median Distance of Piece (mm)	Average Cr Released (ug)	St.Dev	Cr in solid (ug/g dry)	Mass Cr in sample (ug)	Total Cr (ug)	% Leached	Avg % Leached	St.Dev
CS-T5-DI-4 Section 1-A	Chromium 52	84.5	6.92	ug/L	8.56	9.59	33.61	1.03	24.02	2.03	1.97	4.79	1.98	0.00	957.00	699.85	701.88	0.29	0.29	0.00
CS-T5-DI-4 Section 1-B	Chromium 52	85.6	6.92	ug/L	8.66	9.69	33.51	1.03	23.82	2.04	1.98	4.79			963.00	704.24	706.28	0.29		
CS-T5-DI-4 Section 2-A	Chromium 52	111	6.92	ug/L	8.54	9.56	33.55	1.02	23.99	2.66	2.61	14.19	3.62	1.01	910.00	659.02	661.68	0.40	0.57	0.16
CS-T5-DI-4 Section 2-B	Chromium 52	183	6.92	ug/L	8.58	9.54	33.83	0.96	24.29	4.45	4.63	14.19			884.00	602.53	606.98	0.73		
CS-T5-DI-4 Section 3-A	Chromium 52	133	6.92	ug/L	8.56	9.51	33.71	0.95	24.2	3.22	3.39	23.68	3.79	0.41	953.00	642.80	646.02	0.50	0.57	0.07
CS-T5-DI-4 Section 3-B	Chromium 52	193	6.92	ug/L	8.60	9.67	32.96	1.07	23.29	4.49	4.20	23.86			916.00	695.89	700.38	0.64		
CS-T5-VZ-2 Section 1-A	Chromium 52	84.9	6.92	ug/L	8.63	9.01	33.66	0.38	24.65	2.09	5.51	6.89	4.77	0.74	940.00	253.61	255.70	0.82	0.74	0.08
CS-T5-VZ-2 Section 1-B	Chromium 52	71.6	6.92	ug/L	8.71	9.14	33.33	0.43	24.19	1.73	4.03	6.89			864.00	263.78	265.51	0.65		
CS-T5-VZ-2 Section 2-A	Chromium 52	239	6.92	ug/L	8.59	9.59	33.65	1.00	24.06	5.75	5.75	16.34	5.60	0.15	957.00	679.47	685.22	0.84	0.81	0.03
CS-T5-VZ-2 Section 2-B	Chromium 52	228	6.92	ug/L	8.73	9.71	33.10	0.98	23.39	5.33	5.44	16.34			966.00	672.14	677.48	0.79		
CS-T5-VZ-2 Section 3-A	Chromium 52	255	6.92	ug/L	8.51	9.54	33.81	1.03	24.27	6.19	6.01	22.99	6.27	0.27	934.00	683.03	689.22	0.90	0.93	0.03
CS-T5-VZ-2 Section 3-B	Chromium 52	273	6.92	ug/L	8.60	9.62	34.05	1.02	24.43	6.67	6.54	22.99			947.00	685.82	692.49	0.96		
T10HCS1-3 VZP Section 1-A	Chromium 52	25.1	6.92	ug/L	8.57	9.64	33.36	1.07	23.72	0.60	0.56	2.24	0.50	0.06	567.00	430.75	431.35	0.14	0.12	0.01
T10HCS1-3 VZP Section 1-B	Chromium 52	18.8	6.92	ug/L	8.59	9.60	33.37	1.01	23.77	0.45	0.44	2.24			563.00	403.73	404.17	0.11		
T10HCS1-3 VZP Section 2-A	Chromium 52	27.6	6.92	ug/L	8.70	9.50	33.65	0.80	24.15	0.67	0.83	10.93	0.82	0.01	603.00	342.50	343.17	0.19	0.20	0.00
T10HCS1-3 VZP Section 2-B	Chromium 52	16.2	6.92	ug/L	8.60	9.08	33.14	0.48	24.06	0.39	0.81	10.93			572.00	194.94	195.33	0.20		
T10HCS1-3 VZP Section 3-A	Chromium 52	57.1	6.92	ug/L	8.53	9.52	33.94	0.99	24.42	1.39	1.41	23.66	1.27	0.14	736.00	517.33	518.73	0.27	0.24	0.03
T10HCS1-3 VZP Section 3-B	Chromium 52	46.4	6.92	ug/L	8.73	9.71	33.57	0.98	23.86	1.11	1.13	23.66			752.00	523.24	524.35	0.21		
T17LCS2-6 DIW Section 1-A	Chromium 52	25	6.92	ug/L	8.86	9.82	33.99	0.96	24.17	0.60	0.63	3.49	0.64	0.01	636.00	433.50	434.10	0.14	0.14	0.00
T17LCS2-6 DIW Section 1-B	Chromium 52	27.8	6.92	ug/L	8.61	9.62	33.42	1.01	23.8	0.66	0.66	3.49			633.00	453.92	454.59	0.15		
T17LCS2-6 DIW Section 2-A	Chromium 52	30.3	6.92	ug/L	8.67	9.79	33.82	1.12	24.03	0.73	0.65	12.28	0.63	0.02	609.00	484.28	485.00	0.15	0.15	0.00
T17LCS2-6 DIW Section 2-B	Chromium 52	23.1	6.92	ug/L	8.63	9.57	34.16	0.94	24.59	0.57	0.60	12.28			605.00	403.78	404.35	0.14		
T17LCS2-6 DIW Section 3-A	Chromium 52	48	6.92	ug/L	8.64	9.64	33.91	1.00	24.27	1.16	1.16	22.46	1.27	0.11	613.00	435.23	436.39	0.27	0.31	0.05
T17LCS2-6 DIW Section 3-B	Chromium 52	60	6.92	ug/L	8.62	9.67	33.82	1.05	24.15	1.45	1.38	22.46			537.00	400.33	401.78	0.36		
Blank-1	Chromium 52	ND	6.92	ug/L																
Blank-2	Chromium 52	ND	6.92	ug/L																

Legend:

Solution concentrations and sam
Vial tare mass, sample mass and
Sample mass (wet) added to vial
Volume of water added to vial co
Total mass of species released i
Mass of species released per gra
Median Distance of piece taken f
Average release of species from
Content of species measured by
Mass of the species present in th

col U = col T*0.71* col M
Total amount of the species; col
% of species leached calculation

col W = col O/col V

Avg % leached of species from t

A.2

Short Term Leaching Sample Size Calculations

Monolith ID	Distance of edge of piece C1 from wall (mm)	Distance of edge of piece C2 from wall (mm)	Distance of edge of piece C3 from wall (mm)	Width of sample C1 (mm)	Width of sample C2 (mm)	Width of sample C3 (mm)	Half Width of Sample C1 (mm)	Half Width of Sample C2 (mm)	Half Width of Sample C3 (mm)	Mean Distance of Sample from outer wall (mm)	Mean Distance of Sample from outer wall (mm)	Mean Distance of Sample from outer wall (mm)
CS-T5-DI	9.58	18.80	28.56	9.58	9.22	9.76	4.79	4.61	4.88	4.79	14.19	23.68
CS-T5-VZ	13.77	18.91	27.07	13.77	5.14	8.16	6.89	2.57	4.08	6.89	16.34	22.99
T10HCS1-3	4.47	17.38	29.93	4.47	12.91	12.55	2.24	6.46	6.28	2.24	10.93	23.66
T17LCS2-6	6.98	17.57	27.34	6.98	10.59	9.77	3.49	5.30	4.89	3.49	12.28	22.46

Taken from TI-SWCW-010 pg 16.pdf

Width of sample calculated by substracting the distance of the adjacent piece from the measured distance from wall

Half width of each sample, col E to col G/2

Mean distance of sample from outer wall calculated by distance of nearest surface of piece to wall + the half width of the sample:

col K = 0 + col H
col L = col B + col I
col M = col C + col J

Monolith "puck"

Monolith Slice

Central piece sectioned out

Slice sectioned

C1   C2   C3   Remainder

Distance measured and listed in Col B, Col C and Col D

A.3

Appendix B

Monolith Sectioning Data

Monolith Initial Characterization

Monolith ID	CS-T5-DI-4	CS-T5-VZ-2	T10HCS1-3	T14LCS2-5	T17LCS2-6	T21LCS1-4
Mass (g)	278.75	364.69	359.37	388.74	351.47	363.71
Diameter #1 (mm)	49.27	50.1	49.63	49.3	49.9	49.41
Diameter #2 (mm)	49.27	50.11	49.94	49.71	49.74	49.32
Diameter #3 (mm)	49.29	50.23	49.71	49.13	49.86	49.29
Length #1 (mm)	79.37	101.56	101.14	101.33	102.07	101.4
Length #2 (mm)	78.83	103.41	101.28	101.41	101.52	101.57
Length #3 (mm)	79.78	102.61	100.99	101.15	101.78	101.35

Monolith Sectioning

Monolith ID	CS-T5-DI-4	CS-T5-VZ-2	T10HCS1-3	T17LCS2-6
Section A Height (mm)	16.12	15.24	20.07	18.76
Section B Height (mm)	16.17	15.96	19.85	18.7
Section C Height (mm)	16.22	16.35	19.6	18.75
Section D Height (mm)	12.68	16	19.74	18.76
Section E Height (mm)	11.09	32.19	14.41	19.76
Piece C1 distance from wall (mm)	9.58	13.77	4.47	6.98
Piece C2 distance from wall (mm)	18.8	18.91	17.38	17.57
Piece C3 distance from wall (mm)	28.56	27.07	29.93	27.34

Distribution

No. of
Copies

Washington River Protection Solutions&Contractors
EE Brown
KP Lee (AREVA)
RB Mabrouki
JL Mahoney (YAHSG)
PL Rutland
DJ Swanberg
WRPS Documents – TOCVND@rl.gov

Office of River Protection (ORP)
AA Kruger
GL Pyles

INTERA
R Andrews
M Apted
R Arthur
R Senger

Oak Ridge National Laboratory
EM Pierce

Savannah River National Laboratory
AD Cozzi
G Flach
DI Kaplan
CA Langton
DJ McCabe
RR Seitz

No. of
Copies

Pacific Northwest National Laboratory
M Asmussen
DH Bacon
M Bliss
M Bowden
E Buck
VL Freedman
AR Lawter
B Lee
TG Levitskaia
JJ Neeway
KE Parker
CI Pearce
DK Peeler
NP Qafoku
ML Rockhold
JV Ryan
S Saslow
RJ Serne
GL Smith
MMV Snyder
W Um
G Wang
JH Westsik, Jr.
BD Williams
N Washton
SB Yabusaki
Project File
Information Release (pdf)

* All distribution will be made electronically